Quasi-Hinge Beam Element Implemented within the Hybrid Force-Based Method

Ali Biglari[1], Philip Harrison[1*] and Nenad Bićanić[1]

[1] *School of Engineering, University of Glasgow, Glasgow G12 8QQ*

Abstract

This paper describes a new force-based hinge element implemented in the framework of the Large Increment Method (LIM). The element can be of arbitrary cross section and is capable of including inelastic behaviour close to structural hinges. The element formulation can accommodate elasto-plastic strain hardening material behaviour. The solution procedure involves the analysis of elastic and inelastic deformations separately facilitated by splitting of the element length into elastic and inelastic zones. Deformation is calculated by considering inelastic behaviour in the element volume close to both ends of the structural member using an optimum number of integration points in order to achieve good accuracy while maintaining computational efficiency. The predictions of both conventional- and quasi-hinge elements are compared against predictions from Abaqus™. Predictions of the quasi-hinge element show significant improvements over the conventional-hinge method and are shown to converge on the Abaqus™ prediction as the number of monitoring sections in the element is increased.

Keywords: Flexibility Based Method; Large Increment Method; Hybrid Method; Hinge Method; Beam Element

* Corresponding author. Tel: + 44 (0)141 330 4318
E-mail address: Philip.Harrison@glasgow.ac.uk

Glossary of Symbols

The following convention is used in this paper: matrices and second order tensors are written in bold using upper-case symbols, vectors are written using bold lower-case symbols while scalar quantities are written using regular upper and lower case symbols. For convenience a glossary of symbols is given below:

VARIABLES	**DEFINITION**
Ω	*Body domain*
Ω^e	*Elastic body domain*
Ω^p	*Plastic body domain*
Δ	*Deformation vector*
$\boldsymbol{\varepsilon}$	*Strain tensor*
$\boldsymbol{\sigma}$	*Stress tensor*
ε_{ij}	*Strain vector components*
σ_{ij}	*Stress vector components*
ε_N	*Axial strain*
θ_i, θ_j	*Rotation of the ends of the beam element*
θ^e	*Elastic contribution towards rotation at ends of the beam element*
θ^p	*Plastic contribution towards rotation at ends of the beam element*
θ_y	*Section rotation with respect to the y axis*
ϕ_N, ϕ_i, ϕ_j	*Stiffness reduction factors*
μ	*Section ratio*
A	*Element cross section*
A^e	*Elastic cross section*
A^p	*Plastic cross section*
b	*Width of cross section*
b_i	*Body force vector components*
$\boldsymbol{b}$	*Body force vector*
$\boldsymbol{B}$	*Strain-displacement matrix*
$\boldsymbol{\mathcal{B}}$	*Unbalanced load definer matrix*
$\boldsymbol{C}$	*Equilibrium matrix*
$\boldsymbol{C_r^{-1}}$	*Right side inverse matrix*
$\boldsymbol{d}$	*Nodal displacement vector*
$\boldsymbol{D_m}$	*Material constitutive matrix*
$\boldsymbol{\mathcal{D}_m}$	*Section constitutive inverse matrix*
E	*Elastic modulus*
E_t	*Inelastic modulus*
$\bar{f}_i$	*Nodal force component*
f_i	*Elemental force component*
f_s	*Section shape function*
$\boldsymbol{f}_{Se}$	*Section force vector*
f_i^e	*Elastic flexibility matrix components*
δf_i^p	*Inelastic flexibility matrix components*
$\bar{\boldsymbol{f}}$	*Nodal force vector*
$\boldsymbol{f}$	*Elemental force vector*

$\boldsymbol{\delta f}$	*Change in elemental force vector (Unbalanced load vector)*
$\boldsymbol{F_{Se}^{e}}$	*Elastic section flexibility matrix*
$\boldsymbol{F_{Se}^{p}}$	*Inelastic section flexibility matrix*
$\boldsymbol{F}$	*Flexibility matrix*
$\boldsymbol{F^{e}}$	*Elastic flexibility matrix*
$\boldsymbol{F^{p}}$	*Inelastic flexibility matrix*
h	*Element section height*
h_0	*Conjugate gradient modifier*
H_i	*Height of Story i*
$\boldsymbol{I}$	*Identity matrix*
$\boldsymbol{K}$	*Stiffness matrix*
k_0, k_1, k_2, k_3	*Stiffness parameters*
L	*Element length*
L^e	*Elastic element length*
L^p	*Inelastic element length*
L_i^p, L_j^p	*Inelastic length next to end i and j*
M_y	*Moment about y axis*
M_p	*Plastic moment capacity*
M_r^p	*Reduced plastic moment capacity*
M_i, M_j	*Moments at both i, j ends*
n_u	*Nodal degree of freedom number*
n_f	*Elemental degree of freedom number*
N	*Axial force*
N_y	*Section axial strength capacity*
$\boldsymbol{N}$	*Shape function matrix*
$\boldsymbol{p}$	*External load vector*
$\boldsymbol{Q(x)}$	*Section force definition matrix*
S_c	*Shape calibration factor*
$\boldsymbol{s}$	*Search direction vector*
s	*Boundary surface*
s^e	*Elastic boundary surface*
s^p	*Plastic boundary surface*
t_i	*Surface traction force components*
$\boldsymbol{t}$	*Surface traction force vector*
u_i	*Displacement vector components*
$\boldsymbol{u}$	*Deformation vector*
$\boldsymbol{u^{e}}$	*Elastic deformation vector contribution*
$\boldsymbol{u_i^p, u_j^p}$	*Inelastic deformation vector contributions at either end of element*
x_i	*Local coordinate system*
x	*Coordinate aligned with beam length*
Δx	*Displacement shift in x direction*
z	*Distance from the neutral plane*
Δz	*Displacement shift in z direction*
Z	*Force shape function*
$A^*, B^*, C^*, a_1, a_2, b_1, b_2, c_1$	*Dummy Variables*

1. Introduction

The possible occurrence of inelastic deformations when a structure experiences either earthquake or blast loading, can be a significant concern when designing structures. Reducing the computational time associated with modelling and analysis of inelastic structures is an important goal in structural engineering. Generally, inelastic behaviour in frame structures can be studied using two main approaches (i) the Distributed Inelastic Method (DIM), which can be further subdivided into techniques using either customised fibre elements or, more commonly, using continuum elements and (ii) the Concentrated Inelastic Method (CIM). In the fibre-based DIM, each structural member in the frame is modelled by numerous fibres along the length and over the cross section of each element. The fibre-based DIM enables both stress and strain to be determined along the length and through the thickness of the structural member during an analysis. This permits calculation of the gradual spread of inelastic behaviour over the member cross-section and length as deformation proceeds. The fibre-based DIM can provide an accurate solution, enable tracking of phenomena such as cracking and residual stress while being much less demanding in terms of computational resource than a typical full general DIM based on continuum elements. Nevertheless, the computational cost of even the fibre-based DIM can still be prohibitive for certain problems. In such cases, a CIM can provide an alternative and faster method when inelastic behaviour is considered. Using this method, a single element with multiple integration points is used to model each structural member.

When a frame structure is subjected to lateral forces above its yielding load, most of the inelastic material response is often observed to be concentrated towards the ends of the frame's structural members. This observation has prompted the development of the CIM (also known as the plastic hinge or lumped inelastic method). The latter is a computationally efficient method to represent inelasticity in structural frame members. Along the majority of its length a beam usually remains elastic; it is usually only towards the hinges that the elastic capacity of the beam's section is passed. In the conventional implementation of this method, a zero-length hinge is assumed while the rest of the element's behaviour remains elastic [1]. This implies that, as with the fibre-based DIM, just one beam-column element per structural member can capture the inelastic behaviour of the entire structure. This is in contrast with the continuum-based DIM, which involves numerous distinct elements in modelling each structural member. However, a limitation of the conventional CIM is that inelastic behaviour can only be considered at the very ends of a structural beam member. The method is also incapable

of including gradual plasticisation of the hinges, i.e. the gradual increase in length of the plastic zone near the hinges. The resulting element accuracy is consequently affected.

The displacement-based solution strategy involves minimising the strain energy in a structure. This means the final solution is either equal to, or very slightly higher than the minimum possible theoretical energy for the structure. Consequently, the final numerical prediction is usually a very slight overestimation compared to both the theoretical and also the actual stiffness of the structure [2]. This is the case for all elements implemented using a displacement based solution strategy, including hinge elements [3]. As a consequence two methods of improving the conventional hinge element predictions have been proposed; the first is the 'refined hinge' method which, using a displacement-based approach involves the use of stiffness reduction factors to modify the original elastic stiffness matrix, the second is the 'quasi-hinge' method which involves the implementation of a non-zero hinge length. The results of both methods are closer to the exact answer, compared to the conventional zero-length hinge method. These hinge-based methods can be much more computationally efficient than a conventional DIM [3] while still providing results of satisfactory accuracy for most practical purposes [4-6].

In much of the previous research appearing in the literature, hinge elements based on the CIM have been developed and implemented within the framework of relatively mature displacement-based finite element solution strategies. An issue with these displacement-based solution techniques is error accumulation caused by linearisation; after each load increment or step, an iteration procedure, involving a linearisation process, is conducted to minimise any residual error in the solution. This error increases slightly following each step due to the accumulation of small residual errors that remain following each step [7]. Normally, the convergence criteria of the solution algorithm are set so as to ensure this error is negligible. Still, the accumulated error cannot be completely eliminated using displacement-based solution procedures, such as the Newton-Raphson method [8] and in some unusual cases, can lead to either unacceptable inaccuracies or overly long computation times [7, 9]. In addition, strongly non-linear constitutive behaviours can be difficult to handle using displacement based solution strategies. In extreme cases, nodal forces cannot be determined accurately by direct integration over the whole element length and cross-section [10, 11] because the element deformation is too complex to model using cubic Hermitian shape functions, especially when the inelastic deformation gradient is very steep. In such cases the equilibrium equations will not be fully satisfied [12]. Typical techniques to improve the accuracy of displacement-based solution methods when handling steep deformation gradients in inelastic zones are (i) through mesh refinement, though this necessarily leads to longer computation

times and (ii) through the use of higher order elements which again leads to longer computation times. Thus, the computational efficiency of displacement-based methods can be reduced and numerical instabilities are possible, particularly under cyclic loading [1, 12]. In this case, an alternative approach can be to use a force, rather than a displacement-based solution strategy.

The advantages and disadvantages of both the CIM and the DIM, and also the different relative merits of displacement-based and force-based solution strategies have led to the development and publishing of several open source codes incorporating both hinge elements and distributed inelastic elements using both solution strategies. These are summarised in Table 1.

Table 1. *A summary of available open source code*

Softwares	***Displacement based***		***Force Based***		**Developed by**	**University**
	CIM	*DIM*	*CIM*	*DIM*		
ASKA (1969)	√				Argyris, J. H.	Institut Für Statik Und Dynamik Der Luft-Und
IDARC3D (1984)					Park,Y. J.	State University Of New York At Buffalo
GIFT/IFM (1992)			√	√	Patnaik, S. N.	National Aeronautics & Space Administration
DRAIN3DX (1994)	√	√			-	National Information Service for Earthquake Engineering (NISEE)- University Of California, Berkeley
ASAP (2000)	√	√	√	√	Biglari, A.	Ferdowsi University Of Mashhad
Code Aster (2001)		√			-	EDF Energy Co.
FRAME3D (2004)	√				Krishnan, S.	California Institute Of Technology

The main goal of the current work is to use the CIM to develop a quasi-hinge element within the solution strategy of a force-based Large Increment Method (LIM) rather than a displacement based solution algorithm to involve inelastic behaviour. The LIM is a force-based solution strategy [13] and has been employed as the framework in which to implement the new element.

In order to achieve this goal, a beam-column element formulation is implemented to introduce general bending and axial stiffness effectively in conjunction with a CIM based on Euler-Bernoulli beam theory. Both conventional (zero length hinge) and quasi-hinge (finite length hinge) elements have been implemented here to

allow comparison of predictions from the two methods. Both elements have been formulated with arbitrary general section geometries and to account for elasto-plastic strain hardening material behaviour in LIM [14].

The structure of the rest of the paper is as follows; the first section is a brief outline of the historical development of the CIM using displacement based solution strategies. Next, force based solution strategies are described before focusing on the LIM concept, governing equations and solution procedure. Moving onto the development of the new element, the yield surface definition required in the hinge element formulation is first described; the latter is based on an axial force-moment interaction and is used to define the length of the inelastic zone along the element length in the first solution state. Next, the method used to determine the stiffness matrix, which is determined here without resorting to the usual integration procedure, is discussed. In the final section, four numerical examples are presented. The structures of the first two examples are subjected to only axial forces and demonstrate the ability of the solution procedure in analysing two simple structural problems. Results are compared against both theory and previously published work [7, 14] and serve to demonstrate the accuracy of the underlying LIM code. The final two examples involve the use of the conventional hinge and quasi-hinge elements. The latter are used to analyse the displacement of a continuous beam subject to both axial and bending loads. Predictions of the various methods are critically assessed before concluding the paper.

1.1 Concentrated Inelastic Method: Historical Development

So far, developments of the CIM have all been implemented using a displacement based family of methods, all using the finite element approach, starting from early work by Clough et al. (1965) who considered elastic and plastic behaviour separately [15,16]. Giberson (1967) later developed a basic 2D, or conventional hinge method, consisting of two rotational springs situated at both ends of a linear elastic element in order to model inelastic end zones [16]. Orbison et al. (1982) proposed a three-dimensional beam element incorporating an elasto-plastic hinge, though here shear deformations were neglected [17, 18]. In the late 80s this conventional hinge method was extended to consider axial force and bending moment interactions using plasticity theory. Calibration of the plastic hinge characteristics was found to be important since the latter depends on the section geometry, material behaviour and both the length and number of plastic hinges [1, 19, 20]. The early 90s saw the development of a refined plastic hinge-based element, involving the use of stiffness reduction factors to modify the value of an elastic stiffness matrix, here *I*-shaped element sections were considered [1, 21, 22]. By applying the tangent modulus concept, developed previously by White (1993) [23], gradual plasticisation

behaviour was modelled leading to improved results [4, 5, 24]. Further improvements were made by Attalla et al. (1994) who introduced a non-zero length quasi-hinge model involving a closed-form expression of the element force-deformation response, derived by exact integration of the section deformation [21]. A weakness of this method was found in cyclic loading as the displacement method usually fails when passing beyond the structure's yield point. A displacement control method was implemented to overcome this difficulty [1, 2, 21]. Following this improvement, progress in this field focused on enhancing this technique further still. For example, in certain cases if a large distributed load is imposed along the beam element, inelastic deformation can occur, not just near the beam's two extremities but also nearer the beam's mid-span. In this case, a moving node can be positioned at the calculated location of the mid-span plastic hinge [6]. In a series of papers, Chen and Kim used a refined-hinge method in an attempt to predict a smooth transition from elastic to inelastic behaviour thereby controlling the gradual plasticisation of the structure [18, 25-27] and the ability of the refined plastic hinge method in tracing significant yielding and residual stresses during the imposition of large axial forces was developed by Ziemian and McGuire (2002) [28]. Increasing the number of integration points in either the refined- or quasi-hinge methods can improve accuracy. A refined hinge method with seven integration points along the element length was proposed by Addessi and Ciampi (2007) demonstrating that the integration point closest to the end of the member has the most significant effect on the results [1, 29].

2. Force Based Method

In the force-based method, a force shape function is used to interpolate the sectional force vector components between nodal values, effectively satisfying the equilibrium equation point wise along the length of the beam element. Since the force equilibrium equation is satisfied along the entire length of the element this increases the accuracy of the element and is a significant advantage of the force based solution scheme. This is in contrast to the displacement based method and the hybrid displacement method which both depend on interpolating deformation as the primary variable along the element [30]. The most significant difference between the displacement and force-based methods is caused since the deformation field is more complex and discontinuous compared to the corresponding force field, especially in inelastic regions where the deformation field can have steep gradients which cannot be fully captured using simple interpolation functions (e.g. cubic Hermitian interpolation functions used for beam elements), unless extremely refined meshes or more complex interpolation functions are employed. Further, while the distribution of the internal force vector components is known throughout all the frame elements through the equilibrium equations, the same cannot be said for the

deformation field which is usually estimated using appropriate interpolation functions. These factors have caused a significant reprisal in attempts to formulate force-based inelastic fields and corresponding solution methods [31].

3. Large Increment Method

The principle of complementary potential energy has been an attractive approach for structural analysis in force-based methods because it provides a more accurate flexibility matrix, in contrast to the conventional displacement-based method which is based on the principle of total potential energy, the accuracy of which is affected by the interpolation function and solution procedure [32, 33]. This makes the LIM an attractive numerical procedure with a higher rate of convergence than the displacement-based method. The LIM was first presented by Zhang and Liu (1997) who demonstrated the ability of this method to converge using less elements and time steps compared to the equivalent displacement-based approach [7, 34]. The LIM has been used to analyse structures made of materials with elasto-perfectly plastic behaviour, though so far only for rectangular sections with asymmetric degrees of freedom, conducted by considering the shear force and moment at just one end of the element [14, 35]. Flexibility coefficients describing elasto-perfectly plastic behaviour were proposed by Barham et al. (2005), based on an axial force-moment yield surface [13, 36]. Recent research in this area has focused on modelling inelastic behaviour using a fibre-based DIM for elements incorporating linear strain hardening behaviour under cyclic loading conditions and for arbitrary element sections. The elements were formulated based on J2 flow theory [37].

3.1. The LIM Governing Equations

The governing equations used in the LIM are outlined in this section. Let the structure domain, Ω, be defined by,

$$\Omega = \{(x_i, i = 1,2,3) \in \mathbb{R} |\ x_1 \in [0, l],\ x_2 \in [-b/2, b/2],\ x_3 \in [-h/2, h/2]\} \quad (1)$$

where x_i is the element's local orthonormal co-ordinate system, which convects with the element during displacements and deformations. x_1 is orientated along the beam element length and x_2 and x_3 are transverse to the length. h, b and l define the beam dimensions. The principles of minimum total and complementary potential energy are applied throughout the Ω domain and lead to the equilibrium and the compatibility equations respectively. They can be defined as,

$$\int_{\Omega} \delta\varepsilon_{ij}^{T}.\sigma_{ij}.d\Omega - \int_{\Omega} \delta u_i^{T}.b_i.d\Omega - \int_{s} \delta u_i^{T}.t_i.ds = 0 \quad (2)$$

$$\int_{\Omega} \delta\sigma_{ij}^{T}.\varepsilon_{ij}.d\Omega - \int_{\Omega} \delta b_i^{T}.u_i.d\Omega - \int_{s} \delta t_i^{T}.u_i.ds = 0 \quad (3)$$

where δ indicates a finite increment and u_i defines continuous local element displacement field components, b_i, t_i , are the body force and the external traction components acting on the domain, Ω, and the external domain surface is defined by s. The Cauchy stress components are defined by σ_{ij} and the Cauchy strain components by ε_{ij}. These can be used to determine the LIM force equilibrium and element compatibility equations (the latter provide displacement continuity between elements) [37, 38]. The force shape function $\boldsymbol{Z}$ defines the relationship between the element force vector, $\boldsymbol{f}$, and Cauchy stress tensor , $\boldsymbol{\sigma}$, at each section, i.e.

$$\boldsymbol{\sigma} = \boldsymbol{Z}.\boldsymbol{f} \quad (4)$$

Likewise the Cauchy strain tensor, $\boldsymbol{\varepsilon}$, can be related to the displacement vector, $\boldsymbol{d}$, which contains the nodal displacements, using the strain-displacement matrix, $\boldsymbol{B}$

$$\boldsymbol{\varepsilon} = \boldsymbol{B}.\boldsymbol{d} \quad (5)$$

and as is customary, $\boldsymbol{B}$ can be extracted from the displacement-based shape function, $\boldsymbol{N}$, i.e.

$$\boldsymbol{u} = \boldsymbol{N}.\boldsymbol{d} \quad (6)$$

where $\boldsymbol{u}$ is the usual deformation vector calculated using interpolation functions and nodal displacements. Using these definitions, the principles of minimum total potential energy, Eq. (2), can be re-written as,

$$\left(\int_{\Omega} \boldsymbol{\delta d}^{T}.\boldsymbol{B}^{T}.\boldsymbol{Z}.d\Omega\right).\boldsymbol{f} - \int_{\Omega} \boldsymbol{\delta d}^{T}.\boldsymbol{N}^{T}.\boldsymbol{b}.d\Omega - \int_{s} \boldsymbol{\delta d}^{T}.\boldsymbol{N}^{T}.\boldsymbol{t}.ds = 0 \quad (7)$$

Next, by defining

$$\boldsymbol{C}.\boldsymbol{f} = \boldsymbol{p} \quad (8)$$

and then comparing Eqs. (7) and (8), it is possible to find

$$\boldsymbol{C} = \int_{\Omega^e+\Omega^p} \boldsymbol{B}^{T}.\boldsymbol{Z}.d\Omega \quad (9)$$

and

$$\boldsymbol{p} = \int_{\Omega^e+\Omega^p} \boldsymbol{N}^{T}.\boldsymbol{b}.d\Omega \quad + \int_{s^e+s^p} \boldsymbol{N}^{T}.\boldsymbol{t}.ds \quad (10)$$

where $\boldsymbol{C}$ is the stucture's $n_u \times n_f$ equilibrium matrix, $\boldsymbol{p}$ is the external load vector (a $n_u \times 1$ vector) and $\boldsymbol{f}$ is the internal load vector (a $n_f \times 1$ vector). Here n_u is the number of displacement degrees of freedom and n_f is the number of elemental degrees of freedom for the whole structure.

Looking now at the external energy part of Eq. (3), i.e. the body force and surface traction, by mathematical manipulation it can be shown that

$$\int_{\Omega} \delta b_i^T . u_i . d\Omega - \int_s \delta t_i^T . u_i . ds = \boldsymbol{p}^T . \boldsymbol{d} \tag{11}$$

Note that Eq. (11) is not derived from Eq. (10). Substituting Eqs. (4) and (8) in the principle of minimum complementary potential energy, Eq. (3), leads to,

$$\int_{\Omega} \boldsymbol{\delta f}^T . \boldsymbol{Z}^T . \boldsymbol{\varepsilon} . d\Omega - \boldsymbol{\delta f}^T . \boldsymbol{C}^T . \boldsymbol{d} = 0 \tag{12}$$

Therefore the compatibility equations can be written as,

$$\boldsymbol{C^T} . \boldsymbol{d} = \Delta \tag{13}$$

here Δ is the elemental deformation vector (a part of $\boldsymbol{u}$) and contains the element's axial deformation and the element's rotations at both ends, $\boldsymbol{C}$ and $\boldsymbol{p}$ can be separately defined in both the elastic domain, Ω^e, and the plastic domain, Ω^p, and also over the associated surfaces, s^e and s^p while Δ can be defined as

$$\Delta = \int_{\Omega^e + \Omega^p} \boldsymbol{Z}^T . \boldsymbol{\varepsilon} . d\Omega \tag{14}$$

Eq. (13) is required in order to include the compatibility equation in the structural analysis procedure along with Eq. (8), the force equilibrium equation. Note that simultaneous use of Eqs. (8) and (13) in structural analysis is an unusual step, others have adopted similar approaches e.g. [7] though in that case, a different method of formulating these equations was employed.

3.2. The LIM Solution Procedure

The equilibrium equation, Eq. (9) can be written as follows

$$\boldsymbol{f} = \boldsymbol{C}_r^{-1} . \boldsymbol{p} + \boldsymbol{\delta f} \tag{15}$$

where $\boldsymbol{C_r^{-1}}$ is the right-side inverse of the equilibrium matrix, $\boldsymbol{C}$

$$\boldsymbol{C}_r^{-1} = \boldsymbol{C}^T . (\boldsymbol{C} . \boldsymbol{C}^T)^{-1} \tag{16}$$

The term $\boldsymbol{\delta f} = \boldsymbol{\mathcal{B}}.\boldsymbol{f}$ in Eq. (15) is an unbalanced load vector that has to be eliminated in a numerical iteration process (see Table 2). The unbalanced load vector definer matrix, $\boldsymbol{\mathcal{B}}$**,** is given as

$$\boldsymbol{\mathcal{B}} = \boldsymbol{I} - \boldsymbol{C}_r^{-1}.\boldsymbol{C} \tag{17}$$

where $\boldsymbol{I}$ is a unit matrix of size $n_f \times n_f$. By substituting Eq. (16) in Eq. (13), the compatibility equation can be converted to a simple and effective form, suitable for solution using the LIM where the condition $\boldsymbol{\mathcal{B}}.\Delta = \mathbf{0}$ must hold. The condition $\boldsymbol{\mathcal{B}}.\Delta = \mathbf{0}$ is used during the LIM in order to solve the equilibrium equation, i.e. Eq. (15); by achieving this equality the compatibility equation is automatically satisfied. This effectively means that the term $\boldsymbol{\mathcal{B}}.\Delta = \mathbf{0}$ can be considered as a necessary condition for element compatibility and should be achieved at the local stage for individual elements in order to satisfy the compatibility equation across the whole structure at the global stage. To do this a force vector regulator function, $h_0.\mathbf{s}$, is defined following [13,14] and is used to iteratively modify $\boldsymbol{f}$ until the compatibility criterion, $\boldsymbol{\mathcal{B}}.\Delta = \mathbf{0}$ is satisfied (shown at step 6 of Table 2). The LIM solution procedure is summarized in Table 2, where $\boldsymbol{K}$ is the element stiffness matrix.

Table 2. *The LIM solution procedure*

Large Increment procedure			
1	Make external load vector		$\boldsymbol{p}$
2	Make structural equilibrium matrix		$\boldsymbol{C}$
3	Calculate right-side inverse of equilibrium matrix		$\boldsymbol{C}_r^{-1} = \boldsymbol{C}^T.(\boldsymbol{C}.\boldsymbol{C}^T)^{-1}$
4	Calculate unbalanced load vector definer matrix,		$\boldsymbol{\mathcal{B}} = \boldsymbol{I} - \boldsymbol{C}_r^{-1}.\boldsymbol{C}$
5	Calculate initial element force vector		$\boldsymbol{f} = \boldsymbol{C}_r^{-1}.\boldsymbol{p}$
6	Calculate element's deformation vector		$\Delta = \boldsymbol{K}^{-1}.\boldsymbol{f}$
	6.1 Control structure compatibility	Yes>Go to 7	$\boldsymbol{\mathcal{B}}.\Delta = \mathbf{0}$
	6.2 Calculate Search direction vector		$\mathbf{s} = -\boldsymbol{\mathcal{B}}.\boldsymbol{K}^{\mathbf{T}}.\boldsymbol{\mathcal{B}}.\Delta$
	6.3 Calculate conjugate gradient modifier,		$h_0 = -\Delta^{\boldsymbol{T}}.\mathbf{s}.(\mathbf{s}^{\boldsymbol{T}}.\boldsymbol{K}^{-\mathbf{T}}.\mathbf{s})^{-\mathbf{1}}$
	64 Modify elements force vector	Go to 6	$\boldsymbol{f} = \boldsymbol{f} + h_0.\mathbf{s}$
7	Calculate node displacement		$\boldsymbol{d} = (\boldsymbol{C}.\boldsymbol{C}^T)^{-1}.\boldsymbol{C}.\boldsymbol{\delta}$

4. Element Formulation

In this section the formulation of the new hinge element, as implemented in the LIM code, is described. The goal of the theory is to write the element governing equations in terms of the nodal and elemental degrees of freedom, effectively determining the stiffness matrix, $\boldsymbol{K}$ or equivalently finding the flexibility matrix $\boldsymbol{F}$ (which is the inverse of $\boldsymbol{K}$), i.e. $\boldsymbol{F}=\boldsymbol{K}^{-1}$. These quantities are then passed to the LIM code in order to solve the equilibrium equation (i.e. the algorithm shown in Table 2). The theoretical explanation begins with the assumptions used in formulating the element. The importance of the yield surface in the element formulation is discussed and the particular form of the yield surface used in this formulation is presented. The formulation is designed to separate the elastic and inelastic domains. Finally the element stiffness matrix is written for use in the LIM solution scheme.

4.1. Assumptions

The following assumptions are used to model an Euler-Bernoulli beam-column element,

1. The material is isotropic and homogeneous,
2. The element is not loaded along its span,
3. The element is initially prismatic (i.e. of constant cross section), straight, fully compact and sufficiently braced (i.e. local buckling is neglected),
4. Effects of warping, distortion and bowing are neglected.

4.2. Governing Equations

In this section, the force based beam-column element formulation is described for a 2D beam element of arbitrary cross section with six nodal degrees of freedom, denoted here as, $\bar{\boldsymbol{f}} = \bar{f}_i$ where $i = 1, \ldots, 6$. It is possible to consider axial force and both end moments, as shown in Figure 1.

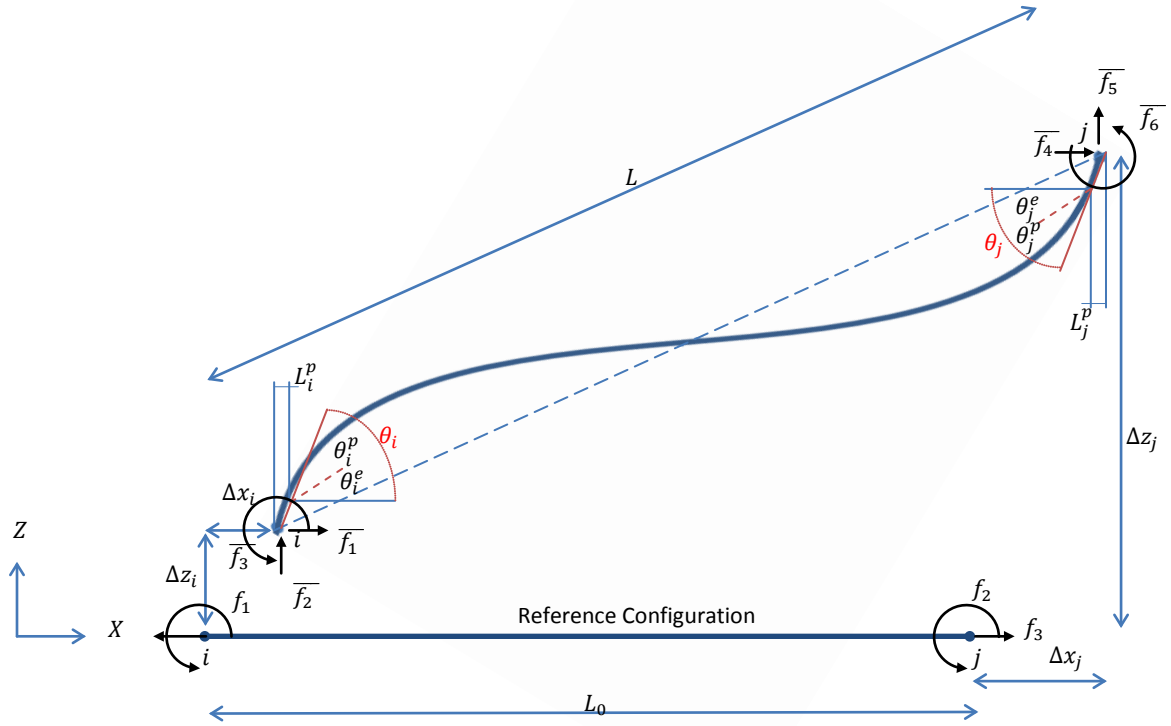

Figure 1.*Beam-Column Element Configuration.*

In Figure 1 θ_i, θ_j are the rotations at the two ends of the element both of which are comprised of elastic and plastic contributions, for example θ_i^e is the elastic contribution and θ_i^p is the plastic contribution to the total rotation at the i^{th} node, Δx and Δz refer to the nodal displacements. The elemental degrees of freedom can be defined for the above element by $\boldsymbol{f} = f_i$ where i =1 to 3. In general, for elasto-plastic behaviour the flexibility matrix, $\boldsymbol{F}$, for an element can be expressed in terms of its elemental degrees of freedom as,

$$\boldsymbol{F} = \int_L \boldsymbol{Q}(x)^T . \left(\boldsymbol{F}_{Se}^e(x) + \boldsymbol{F}_{Se}^p(x) \right) . \boldsymbol{Q}(x) . dx \qquad (18)$$

where $\boldsymbol{Q}(x)$ is a matrix that allows calculation of the section force at any point along the element length, i.e.

$$\boldsymbol{Q}(x) = \begin{bmatrix} 0 & 0 & 1 \\ xL^{-1} - 1 & xL^{-1} & 0 \end{bmatrix} \tag{19}$$

and the section flexibility matrices for both the elastic, $\boldsymbol{F}_{Se}^{e}$,and plastic, $\boldsymbol{F}_{Se}^{p}$ regions of the element are calculated separately as,

$$\boldsymbol{F}_{Se}^{e}(x) = \left(\int_{A^e} \begin{bmatrix} 1 & z \\ z & z^2 \end{bmatrix} . \mathrm{E} . \mathrm{d}A^e \right)^{-1} \tag{20}$$

where E is the Young's modulus, z indicates the distance from the neutral plane and A^e is the part of the element cross sectional area undergoing elastic deformation and

$$\boldsymbol{F}_{Se}^{p}(x) = \left(\int_{A^p} \begin{bmatrix} 1 & z \\ z & z^2 \end{bmatrix} . \mathrm{E}_t . \mathrm{d}A^p \right)^{-1} \tag{21}$$

where E_t is the inelastic modulus and $A^{\boldsymbol{p}}$is the part of the element cross sectional area undergoing plastic deformation. This procedure allows the element to model any general cross section and also permits the addition of shear stress within the element formulation.

Calculation of the elastic and inelastic domains both along and across the element section using the displacement-based method is more difficult due to a much slower convergence rate than the force based method. For this reason, predefinition of the position of monitoring sections (i.e. the sections containing integration points) along the element length is a popular technique to calculate the stiffness matrix in the displacement-based method. Some researchers define fixed integration points in order to solve the integration, though this comes at the cost of eliminating certain parts of the response due to a lack of resolution in the inelastic domain [29]. In contrast, using the force-based method, the location of the inelastic point can be defined by considering the material's stress-strain or force-moment interaction surfaces. It is therefore possible to define the optimum location of the monitoring sections towards both ends of the element and to subsequently calculate the flexibility matrix (which is require to determine the stiffness matrix, $\boldsymbol{K}$, used in the LIM algorithm, see Table 2). Often this is done by splitting the integration domain into elastic, L^e, and inelastic, L^p, regions which leads to a reduction in the computational time, as shown in Eq. (22) [29];

$$\boldsymbol{F} = \boldsymbol{F}^e + \boldsymbol{F}^p = \int_{L^e} \boldsymbol{Q}(x)^T . \boldsymbol{F}_{Se}^{e}(x) . \boldsymbol{Q}(x) . dx + \int_{L^p} \boldsymbol{Q}(x)^T . \boldsymbol{F}_{Se}^{p}(x) . \boldsymbol{Q}(x) . dx \tag{22}$$

The flexibility matrix, $\boldsymbol{F}$, can also be written in terms of the elastic flexibility matrix components, f_i^e, plus the change caused by inelastic behaviour for each component, δf_i^p, i.e.

$$\boldsymbol{F} = \boldsymbol{F}^e + \boldsymbol{F}^p = \begin{bmatrix} f_0^e & 0 & 0 \\ 0 & f_{11}^e & f_{12}^e \\ 0 & f_{21}^e & f_{22}^e \end{bmatrix} + \begin{bmatrix} \delta f_0^p & 0 & 0 \\ 0 & \delta f_{11}^p & \delta f_{12}^p \\ 0 & \delta f_{21}^p & \delta f_{22}^p \end{bmatrix} \tag{23}$$

here $\boldsymbol{F}^e$ is fixed while $\boldsymbol{F}^p$ changes during the calculation. However, an alternative approach has been implemented in this work; rather than separating the flexibility matrix, as shown in Eq. (22), here the deformation vector, $\boldsymbol{u}$, is separated into elastic, u_e and inelastic, u_p parts. This change in procedure reduces computation time because given the exact deformation vector components, u_i, the correct flexibility matrix, $\boldsymbol{F}$, can be calculated without recourse to the computationally expensive integration procedure shown in Eq. (22). This new procedure first requires the calculation of $\boldsymbol{u}$, and from there, $\boldsymbol{K}$ (and therefore $\boldsymbol{F}$) can be determined.

To calculate deformation vector, $\boldsymbol{u}$, it is first required to calculate the section deformation vector, $\boldsymbol{f_{Se}}$ from the section force components using

$$\boldsymbol{f}_{Se} = \int_A \boldsymbol{D}_m \,.\, \boldsymbol{\varepsilon}.\, dA \tag{24}$$

or,

$$\begin{bmatrix} N \\ M_y \end{bmatrix} = \int_A \begin{bmatrix} 1 & z \\ z & z^2 \end{bmatrix} .\, \mathrm{E(z)}.\, \begin{bmatrix} \varepsilon_N \\ \theta_y \end{bmatrix} .\, \mathrm{dA} \tag{25}$$

where $\boldsymbol{D}_m$ is the constitutive matrix and $\boldsymbol{\varepsilon}$ is the strain vector on the element section. N is the magnitude of the axial force and M_y indicates the magnitude of the moment about the y axis acting on the section (see Figure 1). Once again z indicates the distance from the neutral plane, ε_N indicates the axial strain and θ_y is the total section rotation angle about the y axis. Eq. (24) can be re-written as,

$$\boldsymbol{\varepsilon} = \left[\int_A \boldsymbol{D}_m \,.\, dA\right]^{-1} .\, \boldsymbol{f}_{Se} \tag{26}$$

or,

$$\begin{bmatrix} \varepsilon_N \\ \theta_y \end{bmatrix} = \left[\int_A \begin{bmatrix} 1 & z \\ z & z^2 \end{bmatrix} .\, \mathrm{E(z)}.\, \mathrm{dA}\right]^{-1} .\, \begin{bmatrix} N \\ M_y \end{bmatrix} \tag{27}$$

Using the definition of the element deformation,

$$\boldsymbol{u} = \int_L \boldsymbol{Q}(x)^T .\, \boldsymbol{\varepsilon}.\, dx \tag{28}$$

where $\boldsymbol{u}$ is the deformation vector which contains the axial deformation, u_{ij}, and the rotation at both ends of the element $\theta_i$and θ_j. Like Eq. (22), this also involves an integration procedure but here the integration is much

simpler, more accurate and faster to perform compared to the integration procedure involved in Eq. (22); this leads to

$$\boldsymbol{u} = \int_L \boldsymbol{Q}(x)^T . \left[\int_A \boldsymbol{D}_m . dA\right]^{-1} . \boldsymbol{f}_{Se} . dx \tag{29}$$

In order to split this equation into elastic and inelastic domains, as was suggested earlier, it is necessary to define a yield surface. For just the initial deformation state, it is possible to use a simple relationship between axial force and bending moment to obtain this yield surface and from there, a first estimate of the inelastic length. However, as the solution procedure progresses, a more accurate method is required; in this case J2 flow theory is used [47]. In the next section, axial load and bending moment interaction are discussed before the specific relationship used in this method is presented and used as an initial estimate.

4.3. Yield Surface Definition

The main difficulty in developing an elasto-plastic hinge element formulation is in defining a yield surface that can take into account the interaction between the axial force and the bending moment. The most precise method of doing this is through the application of J2 flow theory. However, the process can be greatly simplified and the process significantly accelerated by postulating a simple relationship between axial force and bending moment in the initial element state when using the LIM. A brief review of past research in this area is presented before discussing the approach adopted in this work. A general form for the relationship between the axial force and bending moment for a section can be presented as,

$$\left(\alpha_1 \left(\frac{N}{N_y}\right)^{\alpha_3} + \alpha_2 \left(\frac{M}{M_p}\right)^{\alpha_4}\right)^{\alpha_5} = 1 \tag{30}$$

where N_y is the axial yield force, M_p is the moment plastic strength in the absence of axial loads and α_i are parameters that are usually determined through empirical testing. In order to take account of the section's geometrical effects, Ketter et al. (1955) performed the first calibration of Eq. (30), the result is presented in Eq. (31) [39, 40];

$$\frac{5}{4} . \frac{N}{N_y} + \frac{20}{17} . \frac{M}{M_p} = 1 \tag{31}$$

Similarly, a modified form involving a shape calibration factor, S_c, was proposed by King and Chen (1976). In this case, the calibration was for a linear model with a wide flange section [40];

$$\frac{N}{N_y} + S_c.\frac{M}{M_p} = 1 \tag{32}$$

Although this approach is easy to implement, the effect of a gradual plasticisation is not considered and the resulting yield surface is not able to predict ultimate loads accurately [41]. To do this, the yield surface needs to be calibrated for section geometry and material behaviour and also for bending either in the weak or strong planes. Orbison and McGuier (1982) [17, 40, 42] and the American Institute of Steel Construction (AISC) propose their own calibrated models independently. The AISC suggestion is in two categories as shown in Eqs. (33) and (34), based on the Load and Resistant Factor Design code (AISC-LRFD) bilinear interaction, it can be shown that [41]

$$\begin{cases} \frac{N}{N_y} \geq \frac{2}{9}.\frac{M}{M_p} & , \quad \frac{N}{N_y} + \frac{8}{9}.\frac{M}{M_p} = 1 \\ \frac{N}{N_y} < \frac{2}{9}.\frac{M}{M_p} & , \quad \frac{1}{2}.\frac{N}{N_y} + \frac{M}{M_p} = 1 \end{cases} \tag{33}$$

while for the plastic design code of the AISC, the yield surface is given as [40];

$$\frac{100}{119}.\left(\frac{N}{N_y}\right)^2 + \frac{M}{M_p} = 1 \tag{34}$$

The calibration factor of Orbison and McGuier (1982), which is used to define the yield surface, is given in Eq. (35) [17, 40, 42];

$$\frac{115}{100}.\left(\frac{N}{N_y}\right)^2 + \left(\frac{M}{M_p}\right)^4 + 3.\left(\frac{N}{N_y}\right)^6.\left(\frac{M}{M_p}\right)^2 = 1 \tag{35}$$

Yet another yield surface was proposed by Duan and Chen (1990) based on the ratio, μ, where $\mu =$ (Area of Web)/(Area of Flanges), i.e. [43]

$$\left(\frac{N}{N_y}\right)^{2+1.2\mu} + \frac{M}{M_p} = 1 \tag{36}$$

A similar but simplified model was used by Barham et al. (2005) [36], who used Eq. (37), as an exact definition of the yield surface for an asymmetric element implemented using the LIM which is essentially the same as Eq. (36) with $\mu = 0$.

$$\left(\frac{N}{N_y}\right)^2 + \frac{M}{M_p} = 1 \qquad (37)$$

The effect of the element section geometry and material behaviour on the form of the yield surface is emphasised by the various predictions and is shown in Figure 2 [45, 46].

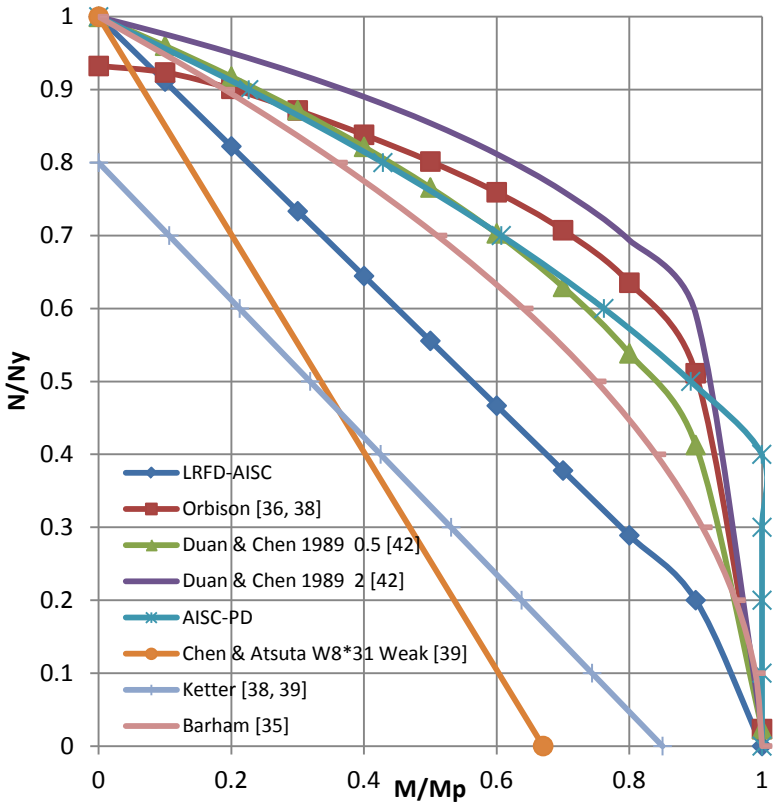

Figure 2. *Yielding surface definitions obtained using models published in the literature.*

It is clear that while a simple approach provides a reasonable first approximation, there is nevertheless a great deal of variation in the various predictions [44]. Here Eq. (37) is considered a reasonable choice to predefine the inelastic length in the initial state of the LIM algorithm for two reasons; (i) its prediction lies centrally among the range of predictions found in the literature, see Figure 2 and (ii) Eq. (37) can be easily rearranged to determine the 'reduced moment plastic strength', M_r^p, which occurs when the section is subjected to an axial force, N, see Eq. (38).

$$M_r^p = \left[1 - \left(\frac{N}{N_y}\right)^2\right].M_p \qquad (38)$$

There are six different possible options for the moment distribution along the element's length, as shown in Figure 3. These distributions can be used to define the inelastic length using the definition of M_r^p given in Eq. (38).

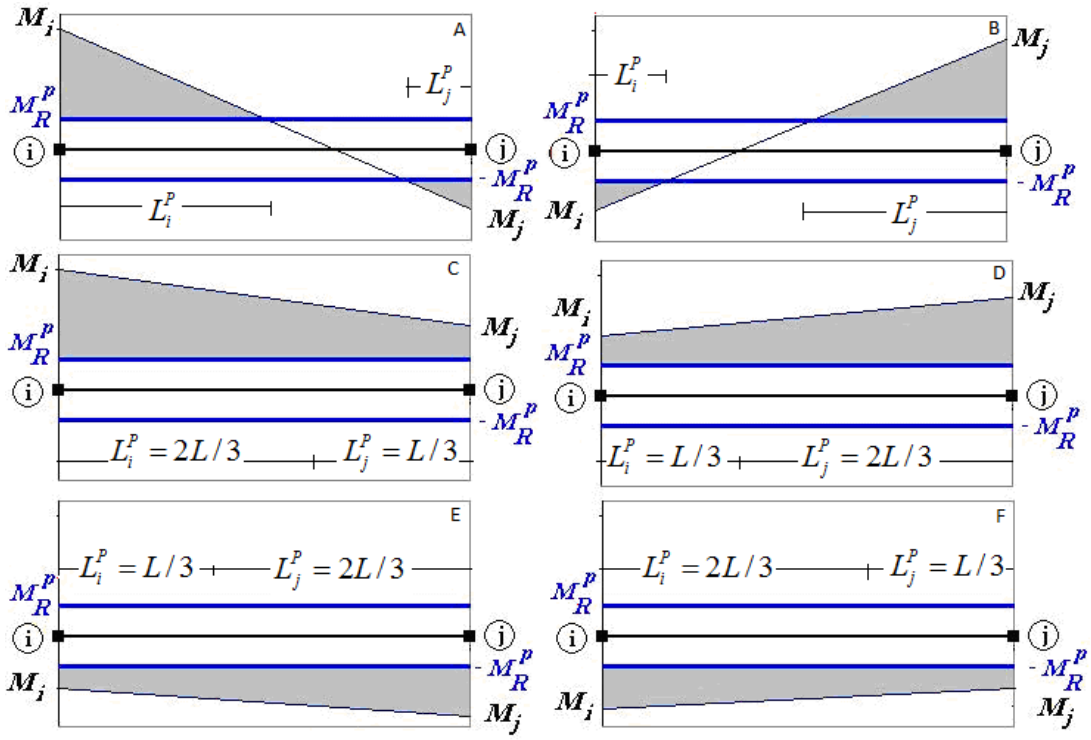

Figure 3. *Moment distribution diagram along the element, note that for cases (C to F) the entire length undergoes inelastic deformation.*

By considering each of these behaviours in turn, the length of the inelastic zones, L_i^p and L_j^p , at both ends of the beam structure, can be determined, i.e.

$$L_i^p = \frac{M_i - M_r^p.sign(M_i)}{M_i + M_j}.L$$
$$L_j^p = \frac{M_j + M_r^p.sign(M_j)}{M_i + M_j}.L \quad (39)$$

where M_i and M_j are the moments acting at the i^{th} and j^{th} ends of the element. To eliminate effect of some certain numerical restrictions the following definitions are also employed,

$$\begin{cases} L^p \geq L & , \quad L^p = \frac{2}{3}.L \\ L^p < 0 & , \quad L^p = \frac{1}{3}.L \\ M_i + M_j = 0 & , \quad L^p = \frac{1}{2}.L \end{cases} \quad (40)$$

L_i^p and L_j^p can be used to split the integration of the deformation field, i.e. Eq. (29) into elastic and inelastic regions. Using this definition leads to Eq. (41),

$$\boldsymbol{u} = \boldsymbol{u}_i^p + \boldsymbol{u}^e + \boldsymbol{u}_j^p \tag{41}$$

where the inelastic deformation contributions $\boldsymbol{u}_i^p, \boldsymbol{u}_j^p$ are defined on the inelastic lengths L_i^p, L_j^p at either end of the element and the elastic contribution, $\boldsymbol{u}^e$, is defined over the remaining elastic length as

$$\boldsymbol{u}_i^p = \int_{L_i^p} \boldsymbol{Q}(x)^T . \boldsymbol{\mathcal{D}}_m . \boldsymbol{f}_{Se} . dx \tag{42}$$

$$\boldsymbol{u}^e = \int_{L-(L_i^p + L_j^p)} \boldsymbol{Q}(x)^T . \boldsymbol{\mathcal{D}}_m . \boldsymbol{f}_{Se} . dx \tag{43}$$

$$\boldsymbol{u}_j^p = \int_{L_j^p} \boldsymbol{Q}(x)^T . \boldsymbol{\mathcal{D}}_m . \boldsymbol{f}_{Se} . dx \tag{44}$$

Also, $\boldsymbol{\mathcal{D}}_m$ is the inverse of the section constitutive matrix and is defined as

$$\boldsymbol{\mathcal{D}}_m = \left[\int_A \boldsymbol{D}_m . dA\right]^{-1} \tag{45}$$

Integration over the whole length of the element enables exact calculation of the nodal displacements and is the most exact way to account for the gradual plasticisation effect. Nevertheless, by reducing the number of monitoring sections in the elastic region, computational efficiency can be improved while still calculating deformation without significant loss of accuracy. However, in order to calculate general deformations while considering the effect of all six independent stress components, the general inelastic behaviour of the element, as determined using J2 flow theory and the consistent tangent operator, must be considered [47].

4.4. Section Behaviour

Accurately locating the neutral plane is a necessary part of accurately determining the section properties. For a general section, the location of the neutral plane and depth of the plastic region can be determined by satisfying the equilibrium equation over the section as follows

$$\boldsymbol{f}_{Se} = \int_A \boldsymbol{D}_m . \boldsymbol{\varepsilon} . dA \tag{46}$$

or

$$\begin{bmatrix} N \\ M_y \end{bmatrix} = \int_A \begin{bmatrix} 1 & z \\ z & z^2 \end{bmatrix} . \mathrm{E(z)} . \begin{bmatrix} \varepsilon_N \\ \theta_y \end{bmatrix} . \mathrm{dA} \tag{47}$$

The explicit answer of Eq. (47) is usually either very complicated or sometimes impossible to formulate. In such cases three possible options have been tried: (i) an approximate method, (ii) a predefined moment-force

couple based on the location of the neutral plane and (iii) a numerical method based on a layered model implemented using both an iterative and a non-iterative approach [48]. The result presented in this paper are based on (iii), the layered model option using an iterative procedure. This method has been found to produce the best performance of these options in terms of both computational time and accuracy.

4.5. Stiffness Matrix

In the current investigation a quasi-hinge element is used within the large-increment force-based method to find the deformation using an integration process, see Eq. (41), and the stiffness matrix is determined from the deformation without recourse to the complex integration step shown by Eq. (22). Instead, now that both $\boldsymbol{u}$ and $\boldsymbol{f}$ are known (see Eq. (41) and Table 2), the stiffness matrix, $\boldsymbol{K}$ can be determined by using certain 'stiffness reduction' factors. These stiffness reduction factors can be computed as both $\boldsymbol{u}$ and $\boldsymbol{f}$ are known and certain constraints on the possible form of $\boldsymbol{K}$ are also known. The element governing equations show the relationship between the force, $\boldsymbol{f}$, and deformation, $\boldsymbol{u}$, and can be written for the symmetric nodal and elemental degrees of freedom as

$$\begin{bmatrix} k_0\phi_N & 0 & 0 \\ 0 & \left(k_1 - \frac{k_2^2}{k_1}(1-\phi_j)\right)\phi_i & \phi_i\phi_j k_2 \\ 0 & \phi_i\phi_j k_2 & \left(k_1 - \frac{k_2^2}{k_1}(1-\phi_i)\right)\phi_j \end{bmatrix} \begin{Bmatrix} u_{ij} \\ \theta_i \\ \theta_j \end{Bmatrix} = \begin{Bmatrix} N \\ M_i \\ M_j \end{Bmatrix} \quad , \quad \boldsymbol{Ku} = \boldsymbol{f} \tag{48}$$

This equation can only be solved for $\boldsymbol{K}$ if the latter takes a specific form. Also, note that the constraint that the length of the element is only affected by axial loads while the rotation of the element is only affected by the bending moments means that four of the components in Eq. (48) are zero. Taken together these constraints mean that the stiffness reduction factors, ϕ_N, ϕ_i and ϕ_j can be defined in Eqs. (49-59) as;

$$\phi_i = \frac{c_1 + b_1.a_2.\phi_j}{b_2.a_1} \tag{49}$$

$$\phi_j = \frac{-B^* \pm \sqrt{B^{*2} - 4A^*C^*}}{2A^*} \tag{50}$$

$$\phi_N = \frac{NL}{u_{ij}AE} \tag{51}$$

where

$$A^* = b_2.a_2.b_1 \tag{52}$$

$$B^* = b_2.c_1 + a_1.b_2.a_2 \tag{53}$$

$$C^* = -M_j.a_1.b_2 \tag{54}$$

and

$$\begin{cases} a_1 = \frac{3}{2}.k_2.\theta_i \quad , \quad b_1 = k_2\left(\theta_j + \frac{1}{2}\theta_i\right) \\ a_2 = \frac{3}{2}.k_2.\theta_j \quad , \quad b_2 = k_2\left(\theta_i + \frac{1}{2}\theta_j\right) \\ c_1 = M_i.b_2 - M_j.b_1 \end{cases} \tag{55}$$

and

$$k_0 = \frac{AE}{L} \quad , \quad k_1 = \frac{4EI}{L} \quad , \quad k_2 = \frac{2EI}{L} \quad , \quad k_3 = \frac{8EI}{L} \tag{56}$$

To eliminate the effect of certain numerical restrictions the following definitions are also employed,

$$\begin{cases} \theta_i = 0 \quad , \quad \theta_j \neq 0 \quad when \quad \phi_i = -\frac{a_2}{c_1}M_i \quad , \quad \phi_j = -\frac{c_1}{b_1 a_2} \\ \theta_i \neq 0 \quad , \quad \theta_j = 0 \quad when \quad \phi_i = +\frac{a_1}{c_1}M_i \quad , \quad \phi_j = +\frac{c_1}{a_1 b_2} \end{cases} \tag{57}$$

and

$$\begin{cases} \theta_i = -2\theta_j \quad when \quad \phi_i = \frac{1}{a_1}M_i \quad , \quad \phi_j = \frac{a_1 M_j}{a_1 a_2 + b_2 M_i} \\ \theta_j = -2\theta_i \quad when \quad \phi_j = \frac{1}{a_2}M_j \quad , \quad \phi_i = \frac{a_2 M_i}{a_1 a_2 + b_1 M_j} \end{cases} \tag{58}$$

and for the axial force

$$u_{ij} = 0 \quad when \quad \phi_N = 1 \tag{59}$$

As a result the exact stiffness matrix can be computed in order to reduce the unbalanced load vector during the LIM iteration procedure (see Step 6 in Table 2). This method replaces calculation of the stiffness matrix based on either eigenvalues or through the complex integration procedure involved in Eq. (22); processes usually employed by previous researchers [13, 48].

5. Numerical Examples

The following examples produced using the LIM code are analysed and compared against both analytical and numerical results. The latter are produced by the commercial implicit finite element code Abaqus™ and provide a numerical benchmark with which to compare the LIM predictions. The performance of the LIM code, and in particular, the predictions of the new elements as implemented within the LIM code, are assessed both in

terms of accuracy and efficiency. The first two examples verify both the performance of the LIM code and the performance of simple truss elements under axial deformation, neither example involves bending moments. The last two examples go on to demonstrate the performance of both a conventional zero length hinge element as well as the new quasi-hinge element when subjected to both axial loads and bending moments. These latter examples involve consideration of the shear stresses in the elements.

5.1. Example I: Column subject to axial load

In the first example, illustrated in Figure 4, a simple column is subjected to a load, *P* (see Table 3), orientated along the axial direction, imposed at Point *C*. The dimensions of the elements are also given in Table 3. The upper and lower ends of the column element are held fixed. The column has an elasto-plastic strain hardening nonlinear material behaviour, see Eq. (60), the parameters of which are given in Table 4 and the column is modelled using just two elements in the LIM simulation (denoted AC and CB in Figure 4).

$$\varepsilon_{11} = \frac{\sigma_{11}}{E} + \frac{\sigma_{11}}{E_p}.\frac{|\sigma_{11}|}{\sigma_0} \tag{60}$$

The resulting displacement at Point C and the internal forces in the two elements are solved using four iterations of the LIM code. A comparison between Abaqus™ predictions presented in reference [7] and the LIM code predictions (displacement at Point C and internal force in element AC) following each increment is given in Table 5, close correspondence (0.000308 per cent difference) is found after just three iterations. The Abaqus™ simulations used 320, 8-node brick elements (C3D8H).

The displacement predicted at Point C versus the load imposed at Point C is plotted in Figure 5A. Similarly, the displacement predicted at Point C versus the internal force predicted in element AC are plotted in Figure 5B. The predictions of the two codes compare very well up to an imposed load of about $5\text{x}10^9$ N, beyond this the predictions begin to diverge [7]. It is interesting to compare the predictions of both codes against analytical predictions for this problem when the imposed maximum load is applied, see Table 6. It is perhaps prudent to note that the Abaqus™ predictions used for this specific comparison are taken from [7] and it is feasible that these results could possibly have been improved. With this note of caution in mind, the results show that the LIM code predictions of both the displacement and internal load are closer to the analytical solution than the predictions of the commercial displacement-based code, Abaqus™.

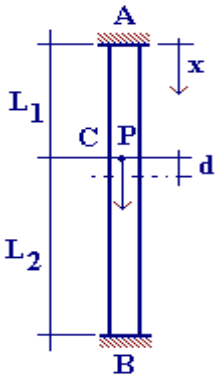

Figure 4. *Example I: Column subject to axial load.*

Table 3. *Geometry and Load parameters.*

Dimensions		Load
L_1 (m)	3	P (N) $1.0\text{x}10^{10}$
L_2 (m)	2	
A (m^2)	0.025	

Table 4. *Non-linear strain hardening material parameters*

	Example I	Example II		Example III	Example IV
		Elastic-linear strain hardening	Elastic-Perfectly plastic		
E (N/m^2)	$1.0\text{x}10^{14}$	$2.0\text{x}10^{11}$	$2.0\text{x}10^{10}$	$2.0\text{x}10^{11}$	$2.0\text{x}10^{11}$
E_t E_t (N/m^2)	$1.0\text{x}10^{13}$	$2.0\text{x}10^{08}$	0	$2.0\text{x}10^{10}$	0
σ_0 (N/m^2)	$1.0\text{x}10^{09}$	$4.0\text{x}10^{07}$	$4.0\text{x}10^{07}$	$2.5\text{x}10^{8}$	$2.5\text{x}10^{08}$

Table 5. *Comparison of LIM and references [7] results for example I*

i_{step}	$F_1\text{x}10^{09}$ (N)	Force difference %	D *(m)*	Displacement difference %
1	5	-9.195947	0.1005	0.02958452
2	5.5	-0.115542	0.09749	0.00002476
3	5.5063452	-0.0000308	0.09746465343090520	0.00000064
4	5.5063621	-0.000001	0.09746645862472853	-0.00000001

This example has also been solved by the LIM code when using an increasing number of loading steps (i_{step} = 5 and 10). The results are presented in Figures 5A and 5B. Increasing the number of load steps has negligible effect on internal force and the nodal displacement prediction. The result demonstrates, at least for the example under consideration, the insensitivity of the LIM code predictions to the number of loading steps, i.e. the code can accommodate large increments in the loading condition with very little loss of accuracy.

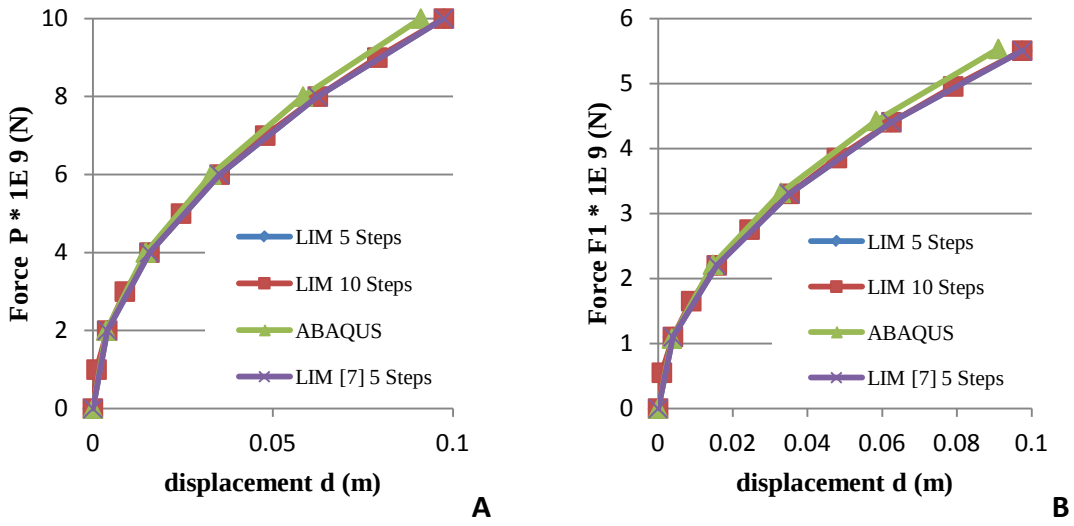

Figure 5. *Comparison of LIM and Abaqus™ results for Example I (A) imposed load versus predicted displacement (B) predicted internal load versus predicted displacement.*

Table 6. *Comparison of LIM and Abaqus™ results for example I compared with analytical solution*

	Results			Error	
	Analytical	LIM	Abaqus	% LIM	% Abaqus
Force, F1, (N)	5496383651.2866	5506362100	5533200000	0.1812167186280	0.669828582
Displacement d, (m)	0.09711245706692	0.09746645862472	0.091068	0.3632034679443	6.224183023

5.2. Example II: Truss-based structure subject to cyclic loading

In Example *II* a truss structure subjected to a cyclic load is analysed. Figure 6A shows the configuration of the structure. Points 3 and 4 are held fixed. Nodes 1 and 2 are free to move in the *x-y* plane. Six elements and four nodal degrees of freedom are used. The truss elements have a bilinear elasto-plastic strain hardening material behaviour, see Eq. (61), the parameters of which are given in Table 4. The cyclic load shown in Figure 6B is applied to Node 1 in the *y* direction. The equivalent Abaqus™ simulation used truss element, T2D2.

$$\begin{cases} \sigma \le \sigma_0 \quad , & \sigma = E\varepsilon \\ \sigma > \sigma_0 \quad , & \sigma = \sigma_0 + E_t(\varepsilon - \frac{\sigma_0}{E}) \end{cases} \tag{61}$$

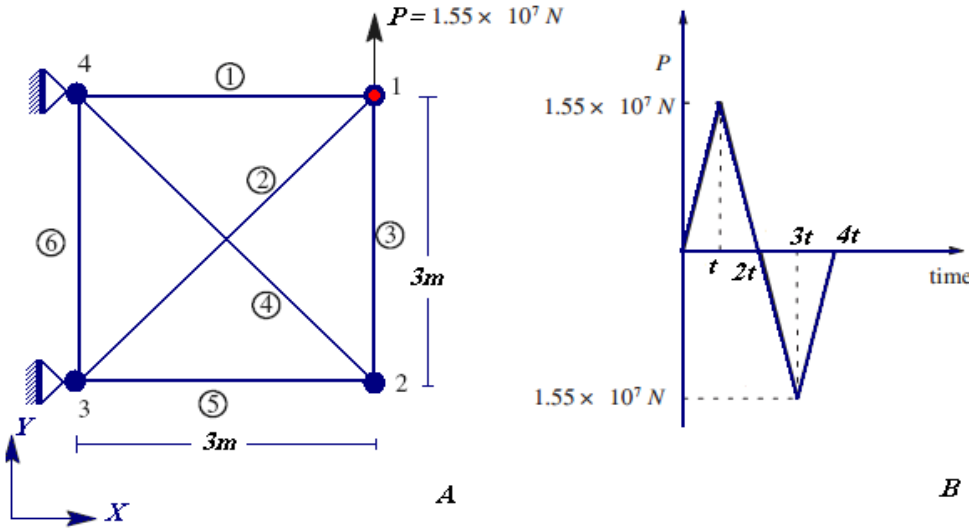

Figure 6. *Example II: Truss-based structure subject to cyclic loading (A) Structure Configuration (B) Cyclic load definition*

The imposed load versus displacement diagram at Node 1, first for an isotropic behaviour next for kinematic behaviour is presented in Figures 7A and 7B. Isotropic behaviour implies the yield surface can change only in magnitude as a function of strain history. In contrast, kinematic hardening behaviour implies the location of the yield surface can be defined as a function of strain history. Ideally a general model should have the capacity to

explain both isotropic (e.g. steel) and kinematic (e.g. concrete) material behaviours [47]. The results show reasonably close correspondence between the predictions of the two codes, though there is a discrepancy in the nodal displacement prediction at high strains.

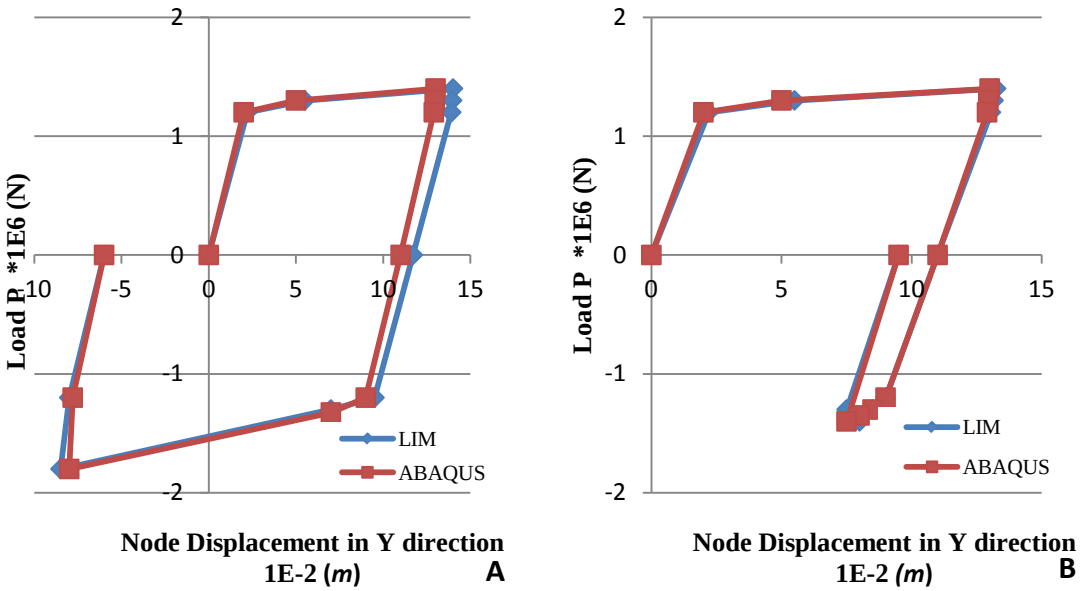

Figure 7. *Comparison of LIM and Abaqus™ result for example II. Load vs nodal displacement (at Node 1) (A) Isotropic behaviour (B) Kinematic behaviour.*

In order to compare results against an analytical solution, the same structure has also been analysed using an elastic-perfectly plastic material behaviour, the parameters of which are given in Table 4. By comparing against the analytical solution both the accuracy and the rate of convergence per iteration of the two codes can be compared. To make a reasonable comparison in terms of the rate of convergence per iteration, the total number of iterations (i.e. the number of load increments multiplied by the number of iterations within each increment) versus solution accuracy for each code can be compared. In Abaqus™ the number of load increments can be set by the user, while the number of iterations within each increment is determined by the Abaqus™ solution algorithm. Thus by changing the number of increments, the user has a limited amount of control over the total number of solutions iterations performed by the code. By varying the total number of iterations and comparing the resulting prediction against the analytical value, some understanding of the sensitivity of the solution accuracy to the total number of iterations can be determined (see Figure 8). The number of iterations performed by the LIM code can also be controlled by various means. In Figure 8 the percentage error in the solutions of the two codes versus total number of iterations performed is plotted. The results suggest that for this particular

example the LIM code converges faster, per iteration, towards the analytical solution than Abaqus™. This suggests possible improvements in computational efficiency; however, given that it is not clear whether the number of calculations per iteration for both the LIM and Abaqus™ algorithms is similar or not, no definitive conclusions regarding the relative computational performance of the two methods can be drawn and closer scrutiny of this point is deferred to future work.

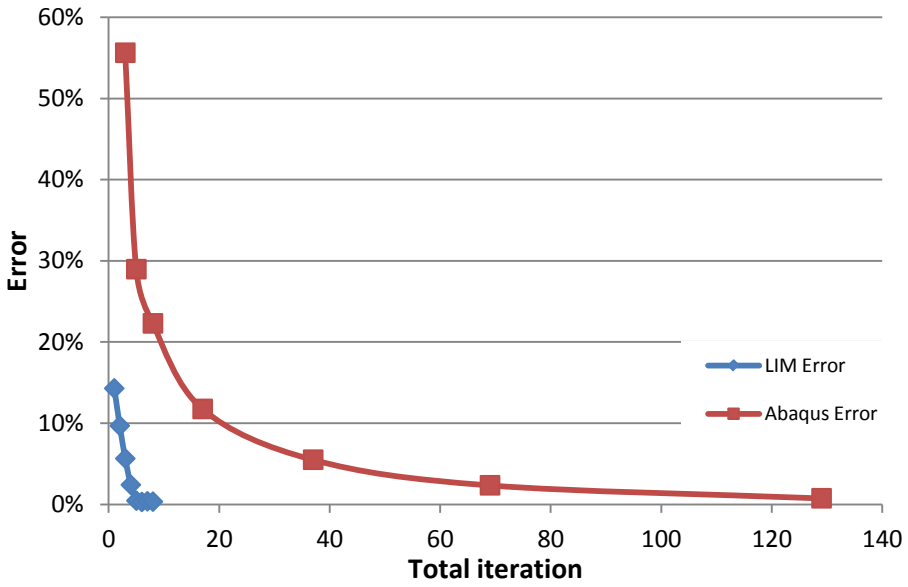

Figure 8. *Percentage error in element force versus total iteration calculated by the LIM and Abaqus™ codes when compared with the analytical solution.*

5.3. Example III: Continuous beam subject to cyclic moment load and axial force

Results from Examples I and II show that predictions of the LIM code for elements loaded in the axial direction (tension and compression) are in close agreement with both Abaqus™ simulations and also with predictions of analytical solutions. Both the example in this section and that in the next section are designed to test the performance of the element for more complex cases involving the simultaneous application of both axial loads and bending moments that result in shear stresses within the beam structure. Shear stresses are considered within the quasi-hinge elements of Example III using a Timosheko formulation [8], i.e. the most common method of incorporating shear stresses within beam elements. In Example IV both Timoshenko and

Reddy [49] formulations have been used in order to examine the effect of the more complex formulation proposed by Reddy [49] on the resulting predictions.

This first example involves a continuous beam structure while the next example demonstrates the method using a frame structure. In each case, the element's predictions are compared against both a conventional hinge element and against Abaqus™. Figure 9A shows a continuous beam with one end fixed (at Point 1) and the other end free to slide without friction along the *x*-direction. Rotations about the *z* and *x*-axes are also prevented along the elements. Three elements have been used to model the structure in the LIM code (the beams are indicated by circled numbers in Figure 9A). The beam is subject to cyclic bending moments at Points 2 and 3 (the points are indicated in red boxes in Figure 9A) while axial cyclic force is applied at Point 4 in the *x*-direction (the loading profile at Points 2, 3 and 4 is shown in Figure 9B. The elements have a bilinear material behaviour, see Eq. (61), the parameters of which are given in Table 4. The equivalent Abaqus™ simulation used 104 beam elements (B21) along the length of the beam structure.

As mentioned, two types of hinge element have been used to analyse the structure of Figure 9; (i) using a zero-length or 'conventional' hinge element and (ii) using the newly developed nonzero-length or 'quasi'-hinge element. In addition two different methods of predicting the yield behaviour of the inelastic end regions can be used in each of these element formulations: (a) a simplified one-dimensional version of J2 flow theory and (b) a full three-dimensional implementation of J2 flow theory. The advantage of using (a), the simplified one-dimensional yield calculation, is that it is much faster than the full three-dimensional calculation (approximately four times as fast when using a conventional hinge method). This approach is only valid if shear stresses are neglected, i.e. for an Euler-Bernoulli beam element formation. In contrast, the advantage of using the full three-dimensional calculation, which considers all six independent components of both the stress and strain tensors, is improved accuracy and the possibility to extend the element formulation to include shear stresses in future work, i.e. Timoshenko as opposed to Euler-Bernoulli formulation.

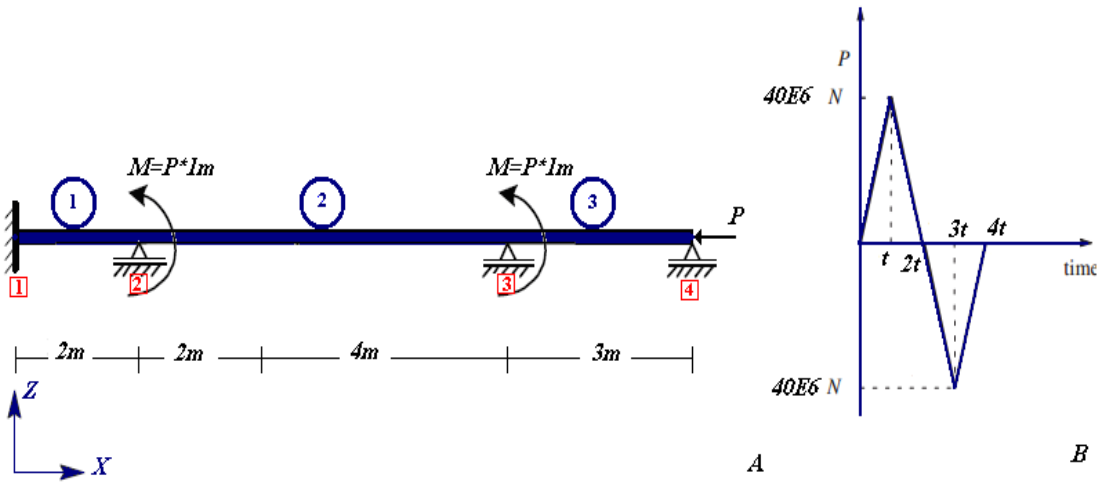

Figure 9. *Example III (A) Structure Configuration (B) Cyclic load definition.*

Figures 10A and 10B show the predictions of the moment versus the rotation angle at Node 3 predicted by Abaqus™ and also by the two types of hinge elements (conventional- and quasi-hinge), both implemented here using the simple one-dimensional yield calculation. Note that the conventional hinge element only uses two monitoring sections, which in this case are positioned at the two extreme ends of the elements. In contrast, the quasi-hinge element can include any number of monitoring sections (a minimum of 3, one for the elastic length and one at either end of the element to represent the inelastic length) and its performance can be optimised by using unequally spaced distances between these monitoring sections, effectively increasing the spatial resolution of the sections in the inelastic regions where deformation gradients are highest. Here a quadratic function has been used to space the monitoring sections within the inelastic zones; 3, 6 and 12 monitoring sections have been used in the quasi-hinge elements, one or two in the elastic mid-span, the rest within the inelastic zones. The aim here is to compare the performance of the conventional and quasi-hinge elements and also to demonstrate the sensitivity of the quasi-hinge element prediction to the number of monitoring sections used in the element. Results in Figure 10A show that using the conventional hinge approach, Method (i), the beam demonstrates a considerably more flexible response than predicted using Abaqus™ since rotation is significantly over-estimated. As expected, the result from the newly developed quasi-hinge element approach, Method (ii), implemented in this first comparison using just 3 monitoring sections, provides a reasonable improvement in accuracy. However, the advantage of the quasi-hinge approach lies in its ability to include any number of monitoring sections. By increasing the number of monitoring sections, the predictions of the quasi-hinge element are seen to approach the Abaqus™ prediction, see Figure 10B.

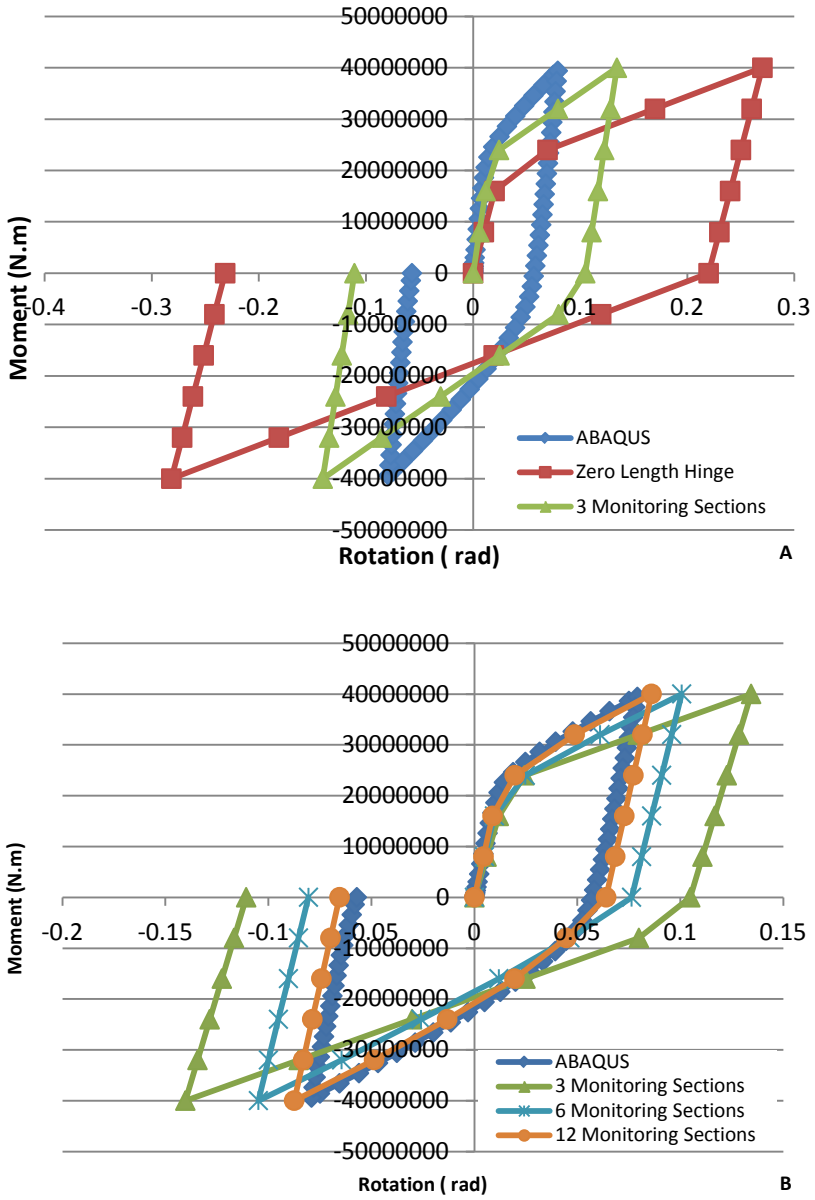

Figure 10. *Comparison of LIM code predictions using three different solution strategies (i-iii) and Abaqus™ for example III: (A) Conventional plastic hinge and quasi-hinge (B)The monitoring section number effect in quasi-hinge method.*

In Figure 11, predictions using Method (b), the full three-dimensional yield surface for the inelastic end regions are shown. Since the effect of the shear deformation was neglected in the element formulation, the results are reasonably similar to those shown in Figure 10B, though following the first loading cycle the results show improved correspondence with the Abaqus™ predictions, giving an almost exact match with Abaqus™ when 12 monitoring sections are used.

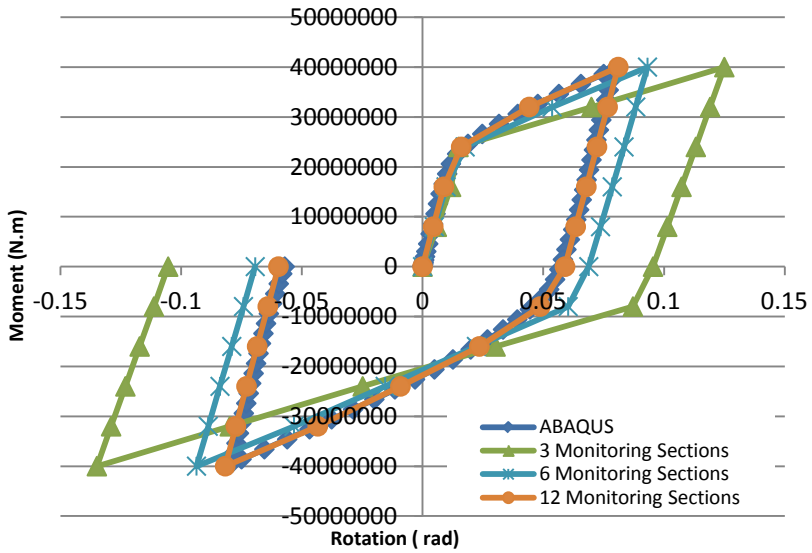

Figure 11. *Comparison of LIM and Abaqus™ result for Example III using a consistent tangent operator [47] showing the effect of the number of the monitoring sections using the quasi-hinge method.*

A further direct comparison of predictions using the simplified yield surface approach, Method (a), and the general 3-dimensional yield surface approach, Method (b), is presented in Figure 12. 12 monitoring sections have been used in both cases. Method (b) is slightly closer to the Abaqus™ prediction than Method (a), although the computational time is increased by about four times. In addition, the prediction from a quasi-hinge element with 180 monitoring sections and using a general three-dimensional yield surface, Method (b), is also shown. The results shown in Figure 12 demonstrate that the prediction converges on the Abaqus™ result, irrespective of the number of monitoring sections used.

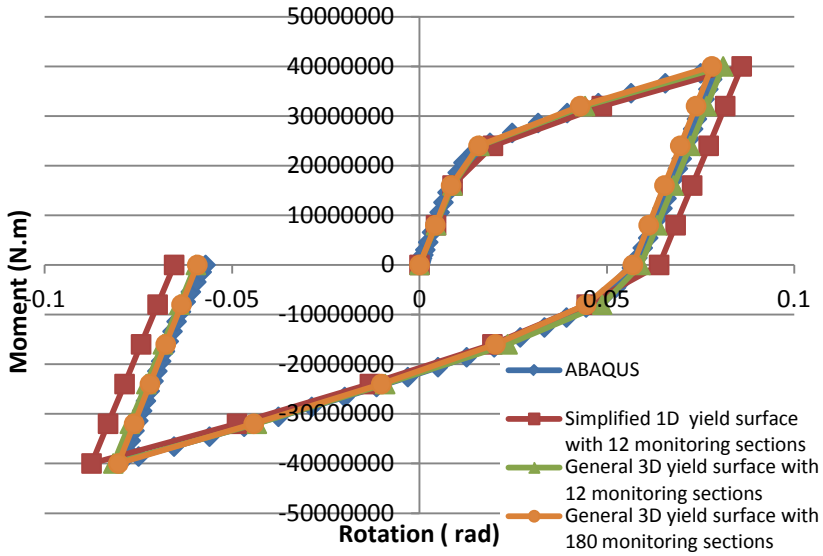

Figure 12. *Comparison of LIM and Abaqus™ result for Example III using the quasi-hinge method.*

In this example, as might be expected the displacement-based approach (Abaqus^{TM}) produces a stiffer prediction compared to the force-based approach (LIM), in fact the two approaches provide a method of estimating an upper and lower bound to the structure's stiffness. It is worth noting that, in terms of safety, underestimating a structure's stiffness is preferably to over estimating the stiffness. As might also be expected, this example suggests that the quasi-hinge element performs significantly better than the conventional hinge element and once again the accuracy of the quasi-hinge method can be significantly improved by increasing the number of monitoring sections, though this comes at the expense of increasing computational cost. Looking again at the rate of convergence of the LIM and Abaqus^{TM} simulations, 40 iterations were required to achieve accuracy with less than 1% error using the force-based LIM algorithm, compared with about 200 iterations for the Abaqus^{TM} simulations. Again, no strong conclusions regarding the relative computational performance of the two methods can be drawn based on this comparison as the number of calculations per iteration for each method is not known, though the reduction in the total number of iterations required by the LIM is encouraging and provides motivation for further research using this method.

5.4. Example IV: Un-braced two story structure subject to monotonic horizontal loading

Results from the previous example show that predictions of the quasi-hinge element are in close agreement with Abaqus^{TM} simulations for a simple single beam structure. This final example is designed to complete the evaluation of the LIM code and quasi-hinge element, i.e. after beginning with a simple column structure and a truss structure to evaluate the LIM algorithm in Examples I and II, a continuous beam structure and finally a frame structure are considered in Examples III and IV in order to investigate the performance of the quasi-hinge element. The same frame structure used in this final example was considered previously by Barham [36] and therefore makes a convenient case study. The quasi-hinge element's predictions are compared here against those of a conventional hinge element implemented in the LIM code, Abaqus^{TM} predictions using hybrid beam elements (B21H) and results published previously by Barham using both their own LIM code (with six beam elements) and standard Abaqus^{TM} beam elements (B23) [36].

Figure 13 shows a single-span, two-story un-braced frame. One of the columns is completely fixed at Point 1 (no translation or rotation is permitted), the other column is fully constrained apart from rotation about the *z*-axis. The frame structure is subjected to a monotonic horizontal load at points 2 and 3. All elements have a rectangular cross section of 0.05m width and 0.2m high and have an elastic perfectly plastic material response, see Eq. (61), the parameters of which are given in Table 4. Six elements have been used to model the structure

in the LIM code while the Abaqus™ simulation used 720 hybrid beam elements (B21H). Here hybrid beam elements are used, as opposed to the standard beam elements used by Barham [36], as predictions using hybrid elements may potentially to be more accurate due to use of an enriched energy function used in implementing their formulation [30].

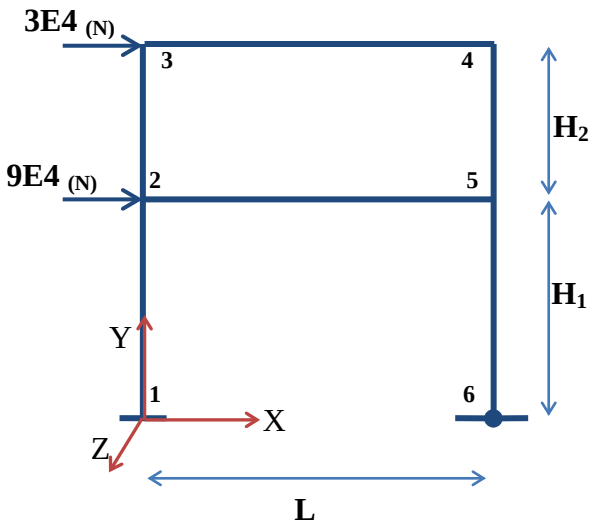

Figure 13. *Structure of Example (H_1=3$_m$, H_2=2$_m$, L=4$_m$).*

As already discussed, two types of hinge element have been used to analyse the structure of Figure 13; (i) the conventional hinge element and (ii) the quasi-hinge element. Figures 14A shows the predictions of the force versus horizontal displacement at Node 2 and Figure 14B shows the predictions of the moment, ($P \times L$; defined in Figure 13), versus angle of rotation at Node 6. In this first case, a Timoshenko formulation has been used to account for shear stress within both the conventional- and quasi-hinge the elements. Predictions by the two hinge elements (conventional- and quasi-hinge) are compared with those made by Abaqus™ and also the published results of Barham [36] in Figure 14. As noted in the previous section, the conventional hinge element uses only two monitoring sections, positioned at the two extreme ends of the element, whereas the quasi-hinge element can include any number of monitoring sections (a minimum of 3, one for the elastic length and one at either end of the element to represent the inelastic length). The conventional hinge approach demonstrates a considerably more flexible response than that predicted using Abaqus™, both the displacement and rotation are significantly over-predicted. As might be expected, the result from the quasi-hinge element, implemented in the first comparison using just 3 monitoring sections, is considerably better than the prediction of the conventional hinge element. The error is reduced from around 50% for the conventional hinge element to about 15% for the quasi-hinge element for both displacement and rotation (see Figures 14A and 14B).

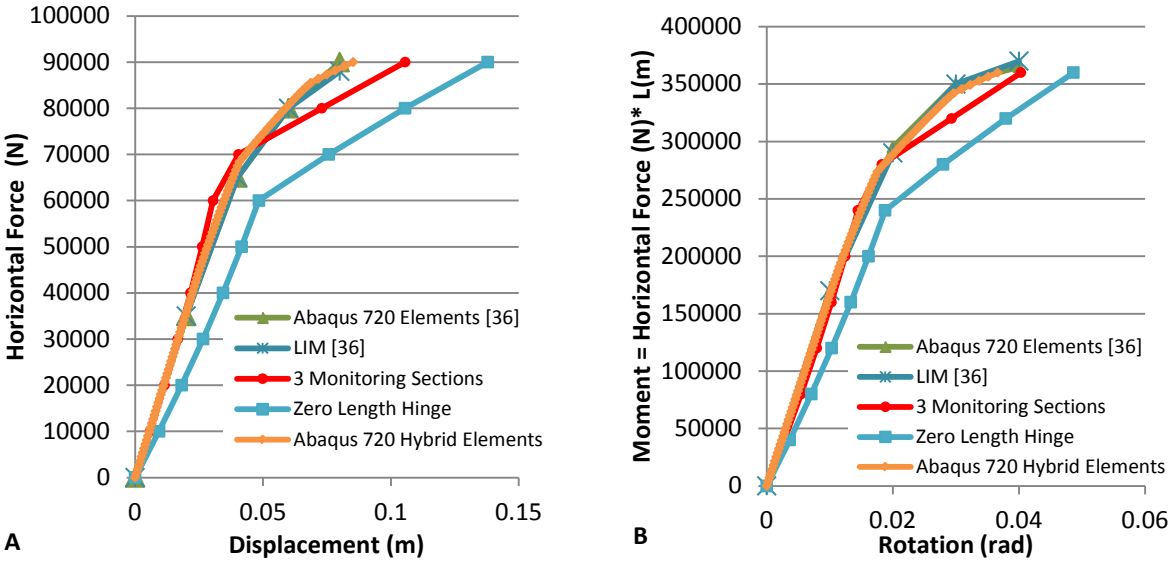

Figure 14. *Comparison of the code predictions and Abaqus™ for example IV: (A) Displacement at Node 2 versus force, P (B) Rotation at Node 6 versus moment (P × L).*

The effect of increasing the number of monitoring sections on the quasi-hinge element predictions is demonstrated in Figures 15A and 15B. Here again, the displacement at Node 2 and the rotation at Node 6 are considered. As demonstrated in the previous example, the advantage of the quasi-hinge approach lies in its ability to include any number of monitoring sections. The predictions of the quasi-hinge element are clearly seen to approach the Abaqus™ prediction, as the number of monitoring sections increases from 3 to 4 to 6. For example, the discrepancy between quasi-hinge and the Abaqus™ predictions reduces to 8.3% (for displacement) and 13.9% (for rotation) using 4 monitoring sections and reduces further still to less than 1% (for displacement) and to about 7.5% (for rotation), when using 6 monitoring sections. This example suggests that the quasi-hinge element performs significantly better than the conventional hinge element and once again, the accuracy of the quasi-hinge method in estimating the rotation angle can be significantly improved by further increases in the number of monitoring sections and also by optimising the monitoring section locations.

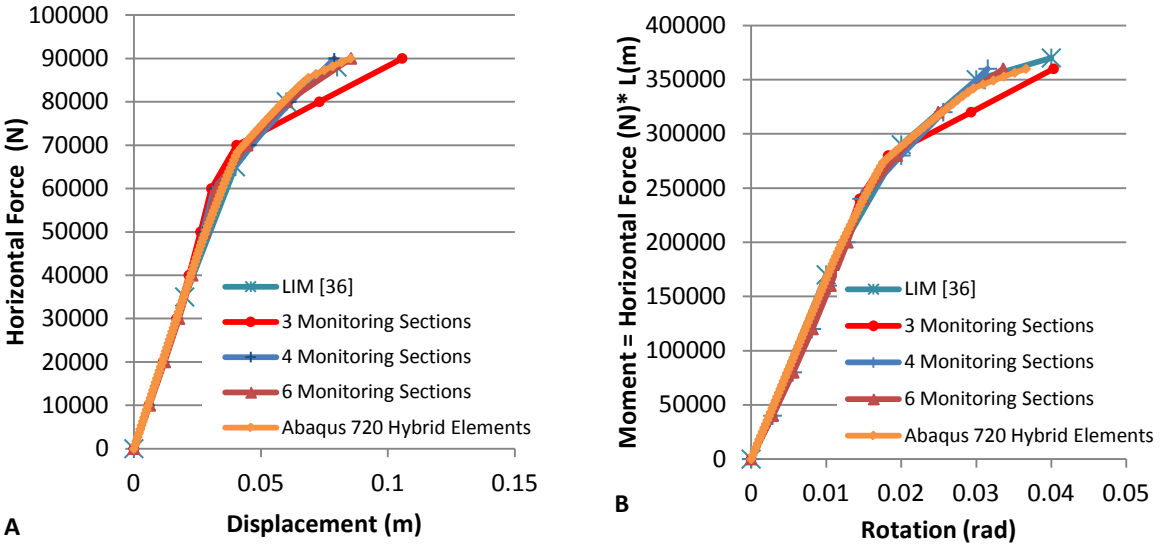

Figure 15. *Comparison of the quasi-hinge and Abaqus™ result for Example IV, using an increasing number of monitoring sections: (A) Displacement at Node 2 versus force P and (B) Rotation at Node 6 versus moment, (P × L).*

It is worth demonstrating the change in accuracy when using a more precise shear stress distribution across the element section, namely by considering different element formulations of the hinge elements. To do this the beam element formulations proposed by Timoshenko [8] and Reddy [49] have both been implemented in the quasi-hinge element. Results in Figure 15 shows that these different formulations have a negligible effect on the accuracy of the displacement predictions, while the accuracy of the rotation prediction changes by about 1%.

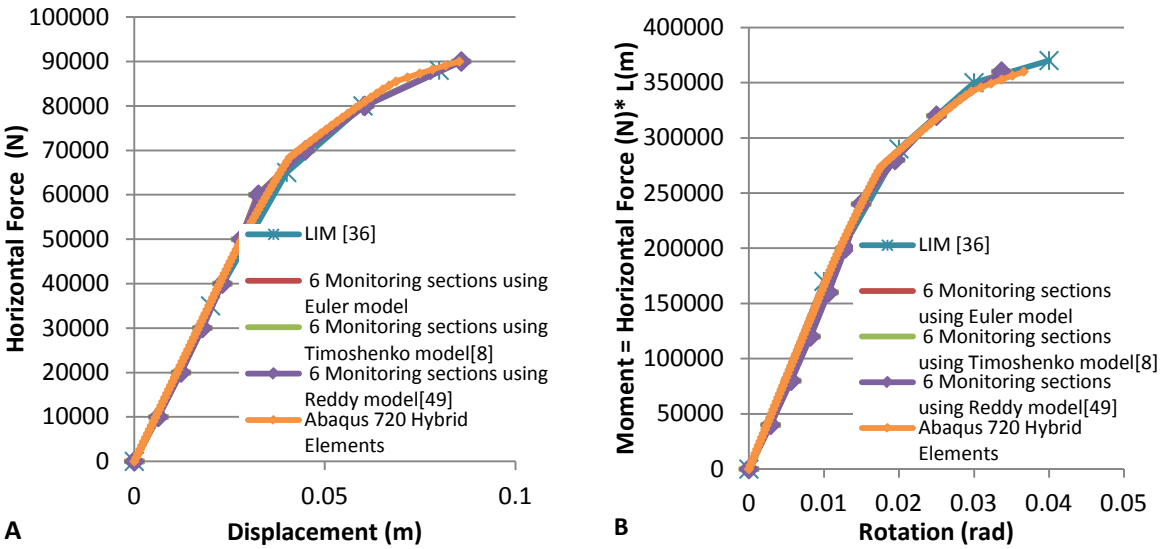

Figure 16. *Comparison of the quasi-hinge and Abaqus™ result for Example IV using the quasi-hinge method and considering different strain distributions over the monitoring sections: (A) Displacement at Node 2 versus force, P and (B) Rotation at Node 6 versus moment, (P × L).*

Finally, looking once again at the rate of convergence of the LIM and Abaqus^{TM} simulations, 27 iterations were required to achieve an accuracy of less than 1% error (for displacement) using the force-based LIM algorithm, compared with about 130 iterations for the Abaqus^{TM} simulations. Again, no strong conclusions regarding the relative computational performance of the two methods can be drawn based on this comparison as the number of calculations per iteration for each method is not known, though the reduction in the total number of iterations required by the LIM provides motivation for further research using this method.

6. Conclusions

A force-based quasi-hinge beam-column element of general section, able to incorporate elasto-plastic linear strain hardening behaviour has been formulated for the first time within the framework of the hybrid LIM solution scheme. The monitoring section definition is implemented based on the elastic and inelastic section response. This procedure reduces the number of integration points, or monitoring sections in the element, required in the force based method to calculate element deformation. The stiffness matrix is then defined directly from the element deformation without a further integration step. The numerical examples demonstrate the good performance of the new hybrid force-based method and the new quasi-hinge element in terms of accuracy, robustness and computational efficiency, at least for the four specific examples considered in this investigation. Further examples and testing are still required for more comprehensive assessment, though these initial results are promising. The element can be extended for general behaviour (e.g., out of plane bending, shear and torsion) and optimised in terms of the number of monitoring sections.

Acknowledgements

We would like gratefully acknowledge financial support from Iran's Ministry of Science, Research and Technology and the Royal Academy of Engineering (ref. 43100168).

References

[1] Lee, C. and Filippou, F. Efficient beam-column element with variable inelastic end zones, *Journal of Structural Engineering, ASCE*, 135(11), (2009) 1310-1319.

[2] Leu, L. Yang, J. Tsai, M. and Yang, Y. Explicit inelastic stiffness for beam elements with uniform and nonuniform cross sections, *Journal of Structural Engineering, ASCE*, 134(4), (2008) 608-618.

[3] Kim, S.E. and Choi, S.H. Practical second-order inelastic analysis for three-dimensional steel frames subjected to distributed load, *Thin-Walled Structures*, 43(1), (2005) 135-160.

[4] Liew, J. White, D. and Chen, W. Second order refined plastic hinge analysis for frame design. Part I, *Journal of Structural Engineering, ASCE*, 119(11), (1993) 3196-3216.

[5] Liew, J. White, D. and Chen, W. Second order refined plastic hinge analysis for frame design. Part II, *Journal of Structural Engineering, ASCE*, 119(11), (1993) 3217-3236.

[6] Wong, M.B. Effects of linearly varying distributed load on the collapse behaviour of frames, *Computers and Structures*, 61(5), (1996) 909-914.

[7] Aref, A. and Guo, Z. Framework for finite-element–based large increment method for nonlinear structural problems, *Journal of Engineering Mechanics, ASCE*, 127(7), (2001) 739-746.

[8] Zienkiewicz, O.C. and Taylor, R.L. The finite element method for solid and structural mechanics, Sixth Ed, Elsevier, Oxford, 2006, 1863 p.

[9]Biglari, A. and Irani, F. Capability of mutation and convergent functions in nonlinear analysis. *Amirkabir Journal of Science and Technology*, 16(63), (2006) 55-61.

[10] Kitipornchai, S. and Al-Bermani, F.G.A. Geometric and material nonlinear analysis of structures comprising rectangular hollow sections, *Engineering Structures*, 10(1), (1988) 13-23.

[11] Teh, L. and Clarke, L.M. Plastic-zone analysis of 3d steel frames using beam elements, *Journal of Structural Engineering, ASCE*, 125(11), (1999) 1328-1337.

[12] Taylor, R. L. Filippou, F. C. Saritas, A. and Auricchio, F. A mixed finite element method for beam and frame problems, *Computational Mechanics*, 31(1-2), (2003) 192-203.

[13] Barham, W.S. Aref, A.J. and Dargush, G.F. Flexibility-based large increment method for analysis of elastic-perfectly plastic beam structures, *Computers and Structures*, 83(28-30), (2005) 2453-2462.

[14]Barham, W.S. Aref, A.J. and Dargush, G.F. On the elastoplastic cyclic analysis of plane beam structures using a flexibility-based finite element approach, *International Journal of Solids and Structures*, 45(22-23), (2008) 5688-5704.

[15] Clough, R.W. Benuska, K.L. and Wilson, E.L. Inelastic earthquake response of tall buildings, *Proceeding of World Conference on Earthquake Engineering*, 2(II), (1965) 68-89.

[16] Giberson, M.F. The response of nonlinear multi-story structures subjected to earthquake excitation, in Civil Engineering Department, (1967) California Institute of Technology, 232 p.

[17] Orbison, J.G. Mcguire, W. and Abel, J.F. Yield surface applications in nonlinear steel frame analysis, *Computer Methods in Applied Mechanics and Engineering*, 33(1-3), (1982) 557-573.

[18] Kim, S. Kim, Y. and Choi, S. Nonlinear analysis of 3d steel frames, *Thin-Walled Structures*, 39 (6), (2001) 445-461.

[19] Hilmy, S.I. and Abel, J.F. Material and geometric nonlinear dynamic analysis of steel frames using computer graphics, *Computers and Structures*, 21(4), (1985) 825-840.

[20] Powell, G.H. and Chen, P.F.S. 3D beam-column element with generalized plastic hinges, *Journal of Engineering Mechanics, ASCE*, 112(7), (1986) 627-641.

[21] Attalla, M. Deierlein, G. and Mcguire, W. Spread of plasticity: quasi-plastic hinge approach, *Journal of Structural Engineering, ASCE*, 120(8), (1994) 2451-2473.

[22] King, W. White, D. and Chen, W. Second order inelastic analysis methods for steel frame design, *Journal of Structural Engineering, ASCE*, 118(2), (1992) 408-428.

[23] White, D.W. Plastic-hinge methods for advanced analysis of steel frames, *Journal of Constructional Steel Research*, 24(2), (1993) 121-152.

[24] Liew, J. White, D. and Chen, W. Notional load plastic hinge method for frame design, *Journal of Structural Engineering, ASCE*, 120(5), (1994) 1434-1454.

[25] Kim, S.E. Park, M.H. and Chio, S.H. Direct design of three-dimensional frames using practical advanced analysis, *Engineering Structures*, 23(11), (2001) 1491-1502.

[26] Kim, S. and Chen, W. Practical advanced analysis for braced steel frame design, *Journal of Structural Engineering, ASCE*, 122(11), (1996) 1266-1274.

[27] Kim, S. and Chen, W. Practical advanced analysis for unbraced steel frame design, *Journal of Structural Engineering, ASCE*, 122(11), (1996) 1259-1265.

[28] Ziemian, R. and Mcguire, W. Modified tangent modulus approach a contribution to plastic hinge analysis, *Journal of Structural Engineering, ASCE*, 128(10), (2002) 1301-1307.

[29] Addessi, D. and Ciampi, V. A regularized force-based beam element with a damage-plastic section constitutive law, *International Journal for Numerical Methods in Engineering*, 70, (2007) 610-629.

[30] Pian, T.H.H. and Wu, C.C. Hybrid and incompatible finite element methods (modern mechanics and mathematics, Chapman & Hall/CRC, New York, (2005), 378 p.

[31] Patnaik, S.N. The integrated force method versus the standard force method, *Computers and Structures*, 22(2), (1986) 151-163.

[32] Hjelmstad, K.D. and Taciroglu, E. Mixed variational methods for finite element analysis of geometrically non-linear, Inelastic Bernoulli–Euler Beams, *Communications in Numerical Methods in Engineering*, 19, (2003) 809-832.

[33] Pellegrino, S. and Van Heerden, T. Solution of equilibrium equations in the force method: a compact band scheme for underdetermined linear systems, *Computers and Structures*, 37(5), (1990) 743-751.

[34] Zhang, C.J. and Liu, X. A large increment method for material nonlinearity problems, *Advances in Structural Engineering*, 1 (2), (1997) 99-109.

[35] Barham, W. Aref, A.J. and Dargush, G.F. A finite element based large increment method for nonlinear structural dynamic analysis, In B.H.V. Topping, (Editor), Proceedings of the Tenth International Conference on Civil, Structural and Environmental Engineering Computing, Civil-Comp Press, Stirlingshire, UK, 2005. doi:10.4203/ccp.81.229

[36] Barham, W.S. Aref, A.J. and Dargush, G. Development of the large increment method for elastic perfectly plastic analysis of plane frame structures under monotonic loading, *International Journal of Solids and Structures*, 42(26), (2005) 6586-6609.

[37] Biglari, A. Harrison, P. Guo, Z. and Bićanić, N. Flexibility based beam element based on large increment method, 8th European Solid Mechanics Conference Proceeding, Graz, Austria, 8-13 July 2012.

[38] Kim, J.K. and Lee, T.G. Failure behaviour of reinforced concrete frames by the combined layered and non- layered method, *Computers and Structures*, 48(5), (1993) 819-825.

[39] Ketter, R.L. Kaminsky, F.L. and Beedle, L.S. Plastic deformation of wide-flange beam-columns, ASCE Trans. 120, (1955) 1019, Reprint No. 91 and 101 (55-5), Fritz Laboratory Reports. 1328.

[40] King, W. and Chen, W. Practical second order inelastic analysis of semi-rigid frames, *Journal of Structural Engineering, ASCE*, 120(7), (1994) 2156-2175.

[41] Steelwork design guide to BS 5950, Vol. 1. Section properties and member capacities, 7th Ed, The Steel Construction Institute (SCI), Berkshire, UK, and The British Construction Steelwork Association Limited (BCSA), London 2000, 554 p.

[42] Chiorean, C.G. A computer method for nonlinear inelastic analysis of 3d semi-rigid steel frameworks, *Engineering Structures*, 31(12), (2009) 3016-3033.

[43] Duan, L. and Chen, W.F. A yield surface equation for doubly symmetrical sections, *Engineering Structures*, 12(2), (1990) 114-119.

[44] Iu, C.K. Bradford, M.A. and Chen, W.F. Second-order inelastic analysis of composite framed structures based on the refined plastic hinge method, *Engineering Structures*, 31(3), (2009) 799-813.

[45] Hsu, C.T.T. Biaxially loaded l-shaped reinforced concrete columns, *Journal of Structural Engineering, ASCE*, 111, (1985) 2576-2629.

[46] Muñoz, P. and Hsu, C. Biaxially loaded concrete-encased composite columns: design equation, *Journal of Structural Engineering, ASCE*, 123(12), (1997) 1576-1585.

[47] Simo, J. and Hughes, T. Computational inelasticity, Springer, Verlag New York, 2000, 392 p.

[48] Neuenhofer, A. and Filippou, F. Geometrically nonlinear flexibility-based frame finite element, *Journal of Structural Engineering, ASCE*, 124(6), (1998) 704-711.

[49] Reddy, J.N. On locking-free shear deformable beam finite elements. *Computer Methods in Applied Mechanics and Engineering*, 149(1-4), (1997) 113-132.